Universidade do Minho
Escola de Engenharia

Rui César Cardoso de Sousa

Synthesis and characterization of electrically conductive bacterial cellulose-polypyrrole composites using alternative synthesis methods.

outubro de 2013

Rui César Cardoso de Sousa **Synthesis and characterization of electrically conductive bacterial cellulose-polypyrrole composites using alternative synthesis methods.** UMinho|2013

Universidade do Minho
Escola de Engenharia

Rui César Cardoso de Sousa

Synthesis and characterization of electrically conductive bacterial cellulose-polypyrrole composites using alternative synthesis methods.

Dissertação de Mestrado em Bioengenharia

Trabalho realizado sob a orientação do
Prof. Doutor Fernando Octávio de Queirós Dourado

outubro de 2013

DECLARAÇÃO

Nome: Rui César Cardoso de Sousa

Endereço electrónico: rccardoso03@gmail.com

Número do Bilhete de Identidade: 13664278

Título dissertação: Synthesis and characterisation of electrically conductive bacterial cellulose-polypyrrole composites using alternative synthesis methods

Orientador: Fernando Octávio de Queirós Dourado

Ano de conclusão: 2013

Designação do Mestrado: Mestrado em Bioengenharia

Universidade do Minho, ___/___/_____

Assinatura: _____

Agradecimentos

"Agradeço ao prof. Doutor Fernando Dourado por me ter dado a oportunidade de integrar este projecto e me ter dado um grande grau de liberdade no que toca à escolha do rumo a dar à investigação."

"Ao Professor Doutor Miguel Gama agradeço por me ter deixado realizar o meu trabalho experimental no seu laboratório e integrar o seu grupo de investigação e ter colaborado com materiais para o desenvolvimento desta investigação."

"Quero agradecer também ao Doutor Vítor Sencadas e ao (brevemente) Doutor Jorge Padrão por todo o apoio, ajuda e conhecimentos que me passaram ao longo desta importante jornada. O meu muitíssimo obrigado por toda a orientação que me deram."

"Ao (brevemente) Doutor Alexandre "States" Leitão por ter sido, para além do Vítor e do Jorge, o primeiríssimo a dar-me babysit no arrancar da minha investigação também um grande e destacado obrigado!"

"A toda a equipa que integra o grupo FUNCARB, os que já lá estavam e os que acabaram por se juntar a nós nesta demanda que é o trabalho laboratorial um grande obrigado por todos os bons momentos que se desenrolaram dentro e fora do lab!"

"Tenho também a agradecer ao professor Doutor Senentxu Lanceros-Méndez a sua simpatia e disponibilidade que demonstrou para me ajudar."

"Quero também agradecer à minha família por todo o apoio que me têm dado ao longo da minha vida académica bem como a motivação e o ânimo necessários à realização deste projecto."

"Quero agradecer também à Joana com um carinho especial por ter sido a companheira de todas as horas e pelo apoio que também me deu ao longo do desenvolvimento deste trabalho, tendo tornado este processo muito mais acessível."

Abstract

As the era of the nanomaterials draws near, the electrically conductive polymeric materials have been receiving increasing attention towards the development of diverse applications in electronics, sensors and actuators. Among these materials, the intrinsic conductive polymers (ICPs) stand out, namely polypyrrole (PPy), an inexpensive and highly conductive ICP (up to 500 $S.m^{-1}$) of facile synthesis, environmentally stability and biocompatibility. By its turn, bacterial cellulose (BC), a biopolymer with highly versatile characteristics, namely chemical purity (0% pectins and hemicelluloses), high crystallinity (95%), low density (1.25 g cm^{-3}), high surface area (37 m^2g^{-1}) as well as excellent mechanical properties (Young's modulus of approx. 15-35 GPa) and low-cost production, have also been drawing a lot of attention**.**

With a combination of these material's promising characteristics in sight, the aim of this work was to obtain electrically conductive BC-PPy composites via *in situ* polymerization. This was achieved by using wet chemical polymerization method. Never-dried and freeze-dried BC thin films were used as the templates for monomer deposition and polymerization. Additionally, an adaptation of the chemical vapour deposition synthesis method was also implemented and tested. The effect of freeze-drying towards the conductivity of the composites was also assessed as it showed promise attending to some published results where the composites are freeze-dried.

Electrically conductive BC-PPy composites exhibiting tailor-made conductivity, which varied depending on the synthesis method selected, were obtained. These conductivities vary between the ranges of $3x10^{-5}$ and $5x10^{-5}$ $S.m^{-1}$ (CVD) and 3-140 $S.m^{-1}$ (WCP), depending on processing method. Additionally, the composites were characterized, alongside the BC and PPy, using a different set of analytical techniques such as conductivity assays, tensile testing, thermogravimetric analyses (TGA), Fourier transform infrared spectroscopy by attenuated reflectance (FTIR-ATR), X-ray diffraction crystallography (XRD) and scanning electron microscopy (SEM). This characterization lead to the conclusion that the BC fibres not only were completely coated by a PPy layer but that a chemical interaction between them also exist.

Resumo

Dada a crescente popularidade dos nanomateriais, os materiais poliméricos electricamente condutores sido alvo de atenção crescente no contexto do desenvolvimento de diversas aplicações no ramo da electrónica, dos sensores e actuadores. Destes materiais, destacam-se os polímeros intrinsecamente condutores (PIC), nomeadamente o polipirrol (PPy), um PIC *low cost*, altamente condutor (≤500 Sm^{-1}), de síntese fácil, e altamente estável no ambiente bem como biocompatível. A celulose bacteriana (CB), um biopolímero com características altamente versáteis, nomeadamente a sua pureza química (0% pectinas e hemiceluloses), elevada cristalinidade (95%), baixa densidade (1,25 $g.cm^{-3}$), grande área superficial (37 $m^2.g^{-1}$), bem como excelentes propriedades mecânicas (módulo de Young de ~15-35 GPa) e produção de baixo custo, também tem demonstrado uma crescente popularidade.

Com a combinação das características promissoras destes materiais em vista, este trabalho visou obter compósitos electricamente conductores de CB-PPy via polimerização *in situ*. Para este fim, para além do método tradicional de polimerização química em solução (PQS), uma adaptação desta técnica foi testada, tendo-se usado BC liofilizada alternativamente à hidratada. Paralelamente, também foi testada adaptação do método de síntese por deposição química de vapor (DQV). O efeito da liofilização na condutividade dos compósitos também foi avaliado, visto que se revelou promissor dado alguns resultados encontrados na literatura em que há liofilização dos compósitos.

Foram obtidos compósitos porosos e não-porosos de BC-PPy com conductividade *tailor-made*, *i.e.*, variável ($3x10^{-5}$ a $5x10^{-5}$ $S.m^{-1}$ (DQV) e 3-140 $S.m^{-1}$ (PQS)) consoante o método de síntese utilizado. Finalmente, os compósitos foram caracterizados, conjuntamente com a CB e o PPy, usando um conjunto de diferentes de técnicas analíticas tais como ensaios de condutividade elétrica, ensaios mecânicos, análise termogravimétrica, espectroscopia de infravermelho por reflectância atenuada, cristalografia por diffracção de raios-X e microscopia eletrônica de varrimento. Esta caracterização permitiu concluir que ocorre o revestimento total das fibras de CB pelo PPy, bem como existe uma interacção química entre a CB e o PPy.

Index

List of Abbreviations

ANOVA – Analysis of variance

BC – Bacterial Cellulose

CVD – Chemical vapour deposition

FTIR-ATR – Fourier transform infrared spectroscopy by attenuated total reflectance

G. xylinus* – *Gluconacetobacter xylinus

HS – Hestrin-Schramm

ICP – Intrinsically conductive polymers

PPy – Polypyrrole

Py – Pyrrole

ρ – Electrical resistivity (Ω.m)

SEM – Scanning electron microscopy

σ – Electrical conductivity ($S.m^{-1}$)

TGA – Thermogravimetric Analysis

WCP – Wet chemical polymerization

XRD – X-Ray diffraction crystallography

Tables Index

Chapter 1 – Introduction

Chapter 2 – Materials and Methods

Chapter 3 – Results and Discussion

Figures Index

Chapter 1 – Introduction

Chapter 2 – Materials and Methods

Chapter 3 – Results and Discussion

Equations Index

Chapter 2 – Materials and Methods

Work contextualization and motivations

Bacterial cellulose (BC), also known as microbial cellulose and bacterial nanocellulose, is a form of cellulose that is chemically similar to the one produced by plants, however, it is secreted by bacteria, namely *Gluconacetobacter xylinus* (G. xylinus). Microbial cellulose displays very interesting properties namely a high Young's modulus, high crystallinity, an exceptional degree of purity and is also biocompatible (Andrade *et al.*, 2010; U.S. Congress, 1993).

These characteristics make cellulose an attractive material for the development of a wide variety of innovative applications in the fields of biomedicine, alimentary supplements and additives, paper production and even in the sound device industry (Andrade *et al.*, 2010). In fact, not only does BC has a high application potential but also there are already some BC-base successful products in the market such as, for example: Biofill (Fontana *et al.*, 1990) wound dressings, introduced in 1990 for clinical trials; the Nata de Coco (Andrade *et al.*, 2010), the food product were the BC was primarily discovered, an alimentary good that is quite popular in the oriental countries and the MDR-R10 headphones developed by Sony, the first audio devices to incorporate bacterial cellulose in its speaker membranes.

Recently, it has been discovered that this material is an attractive insulation matrix for intrinsically conductive polymers (ICPs) such as polypyrrole (PPY) (Wang *et al.*, 2013; Dall'Acqua, 2006). With the era of flexible electronics drawing near, evermore becoming a commercial reality and the continuous and intensive research efforts in order to find a viable and environmental-friendly base-materials, bacterial cellulose is starting to be explored towards the development of this type of applications. The main characteristics of BC that are interesting for this type of applications are its mechanical resilience and elasticity. Some works have already been developed towards this area having already some base composites of BC and PPy been synthesised (Muller *et al.*, 2013; Wang *et al.*, 2013).

The main goal behind this MSc thesis was to obtain electrically conductive composites with, ideally, the electrical conductivity of PPy, while having the mechanical

resilience and elasticity of BC. These composites could potentially be used for the development of flexible electronic devices, as applicable in the most varied fields: from consumer electronics to biosensors (Vaitkuviene *et al.*, 2013; Jin *et al.*, 2000; Vernitskaya and Efimov, 1997). As such, this MSc thesis revolved around the synthesis of BC-PPy composites through the traditional WCP method while implementing one modification, namely, the usage of freeze-dried BC for composites synthesis instead of hydrated BC. Additionaly, an adaptation of Dall'Acqua's method of chemical vapour deposition (Dall'Acqua, 2006) was also implemented and tested towards the synthesis of BC-PPy composites as an alternative method of synthesis.

With said goal in sight, this work focused on the synthesis of electrically conductive composites obtained through the oxidation of BC with ferric chloride and doping with hydrochloric acid followed by the deposition and *in situ* polymerization of PPy on the BC fibrous matrix. As stated above, besides the traditional WCP synthesis method using hydrated BC, two alternative methods were experimented, namely the usage of freeze-dried BC on the WCP method and an adaptation of the CVD. The main reason behind the usage of freeze-dried BC alternatively to hydrated BC was testing the impact of usage of freeze-dried *vs* hydrated BC as the freeze-drying of the samples potentially leads to a high increase of the obtained composites' electrical conductivity as Wang *et al*. (2013) obtained highly conductive BC-PPy composites by freeze-drying them posteriorly to their synthesis

The synthesized samples were characterized in terms of their mechanical, electrical, optical and thermal properties. For this purpose, different techniques such as tensile testing, electrical measurements, SEM, FTIR-ATR, XRD and TGA were used to study the effect of the processing technique towards the electrical performance of the composites.

The thesis work was performed within the FUNCARB (FUNctional CARBohydrates) research group from the IBB (Institute for Biotechnology and Bioengineering) at the Center of Biological Engineering (CEB) of the University of Minho under the supervision of Prof. Doctor Fernando Dourado.

Chapter 1. Introduction

In this chapter, an approach to all the different building blocks that made part of the final objective of this work, namely, the bacterial cellulose (BC) and polypyrrole (PPy), will be made. This consists of a detailed explanation of the materials' properties and the state of the art related to their potential use. An approach to the families of these materials, i.e. the natural and intrinsically conductive polymers' will also be made in order to introduce both the BC and PPy.

Natural polymers

Polymers are a class of chemical compounds that can either be synthetically produced or found in nature being the latter called biopolymers. The biopolymers are a family of polymers that are produced by living organisms through a variety of synthetic mechanisms present in plants, animals and microorganisms (U.S. Congress, 1993). They can either be extracted directly from their source (*e.g.* extracting chitin from crustacean shells) or be produced *in vitro*, by providing to the microorganisms the required nutrients for their biosynthesis (*e.g.* bacterial cellulose).

One of the main treats displayed by the biopolymers is their biocompatibility, which means that these polymers have a predictable rate of adsorption while triggering reduced to null (*e.g.* bacterial cellulose (Andrade *et al.*, 2010)) inflammatory response by the host (U.S. Congress, 1993). This makes the biopolymers good candidates towards the development of biomedical applications as they are safe to use on the human organism.

These compounds are also biodegradable thus being beneficial towards the environment (U.S. Congress, 1993) as they can be degraded by decomposing microorganisms and resulting applications (e.g. bacterially derived thermoplastics) are less harmful towards the environment. In short, biopolymers are not only generally regarded as safe but also environmental friendly.

However, these polymers display some disadvantages, for instance, the extraction of chitin from crustacean shells is a relatively work-intensive extraction process which involves different chemical agents (Arbia *et al.*, 2012). Even when these polymers can be obtained by fermentation, there are also a few complications involved, namely low

product yields and/or low purity which requires cost and time-intensive purification processes (Vroman and Tighzer, 2009; McChesney *et al.*, 2007).

Nonetheless, regardless of the complications associated to the attainment of some of the polymers stated above, there are some examples of these materials that are economically appealing given the fact that their industrial production is potentially cheaper than the production of their synthetic counter-parts. This is due to the fact that the growth media used to culture the producing organisms are generally composed of relatively cheap compounds and other industries by-products (e.g. food industry by-products). One example of a biopolymer that is produced under these circumstances and displays high economic potential is bacterial cellulose, as it will be approached later on this chapter.

A snapshot at the extensive biopolymer family obtained from natural compounds can be seen on **Table 1.1** below).

Table 1.1 – A brief list of the existent natural polymers (U.S. Congress, 1993)**.**

Polyesters	**Polysaccharides (origin: bacteria)**
Polyhydroxyalkanoates	Xanthan
Polylactic acid	Dextran
	Gellan
Proteins	Levan
Silks	Curdlan
Collagen/gelatin	Polygalactosamine
Elastin	Bacterial cellulose
Resilin	
Adhesives	**Polysaccharides (origin: fungi)**
Polyamino acids	Pullulan
Soy, zein, wheat gluten,	Elsinan
casein, Serum albumin	Yeast glucans
Lipid/Surfactants	**Polysaccharides (origin: plants/algae)**
Acetoglycerids, waxes, surfactants	Starch (amylose/amylopectin)
Emulsan	Cellulose
	Agar
Polyphenols	Alginate
Lignin	Carrageenan
Tannin	Pectin
Humic acid	Konjac
	Various gums (e.g. guar, xanthan)
Specialty polymers	
Shellac	**Polysaccharides (origin: animals)**
Poly(γ-glutamic acid)	Chitin/chitosan
Natural rubber	Hyaluronic acid

Among the plethora of existing biopolymers, bacterial cellulose displays a promising potential in terms of application given its interesting physical-chemical properties. This research work is dedicated to the study of this biopolymer's properties and its potential applications as it will be detailed below in the next sub-chapter.

Bacterial Cellulose

Cellulose, primarily known for being a basic structural component in plant cell walls, is the most abundant natural resource on Earth (Encyclopaedia Britannica, 2012). Cellulose displays almost an endless set of applications in wide scope of research fields, such as biomedical applications, electronic components and biofuels. It is also used industrially, as a raw material, in the production of paper, food additives, among other purposes (Andrade *et al.*, 2010). This biopolymer comprises a large number D-glucose monomers, between the hundreds and the tens of thousands, connected together via β(1→4) bonds thus making it one of the reasons why cellulose is not easily degraded in human organism as it lacks the enzymes of cellulases which hydrolyse this linkage (Miyamoto *et al.*, 1989).

Apart from its presence in the structural composition of plants, cellulose is also biologically synthesized by a restricted group of bacteria of the *Acetobacter*, *Pseudomonas*, *Rhizobium* and *Sarcina* genuses, being the *Sarcina* the genus of Gram-positive bacteria that biosynthesizes cellulose (Jonas and Farah, 1998). Despite the aforementioned genuses of bacteria that biosynthesize cellulose, *Gluconacetobacter xylinus*, described in 1886 by Brown (Brown, 1886), is the most studied being its cellulose biosynthesis machinery and culture conditions are fully characterized, being the most commonly used bacteria in cellulose production.

This bacterial-synthesized cellulose, globally referred to as bacterial cellulose (BC), microbial cellulose or bacterial nanocellulose, displays very similar physicochemical properties compared to plant cellulose, being its degree of polymerization, which is averagely 3 fold lower than plant cellulose's, and its fibre diameter, which is comprised in the nanometric scale while plant cellulose fibres are comprised in the micrometric scale (Jonas and Farah, 1998). Another major different between these two forms of cellulose is that BC is chemically pure (Andrade *et al.*, 2010), contrarily to plant cellulose,

since it's secreted by the bacteria to the culture medium free of pectins, hemicelluloses and lignin.

Due to a promising set of properties, namely its biocompatibility and physicochemical properties, being chemically pure and easily produced by bacterial culturing, BC has been the subject of increasing attention from both research groups and industrial companies (Andrade *et al.*, 2010) as it can be seen in **Figure 1.1** where this growing interest in bacterial cellulose is demonstrated by reporting the evolution of the number of patents and publications related to this biopolymer and its possible applications between 1990 and 2008.

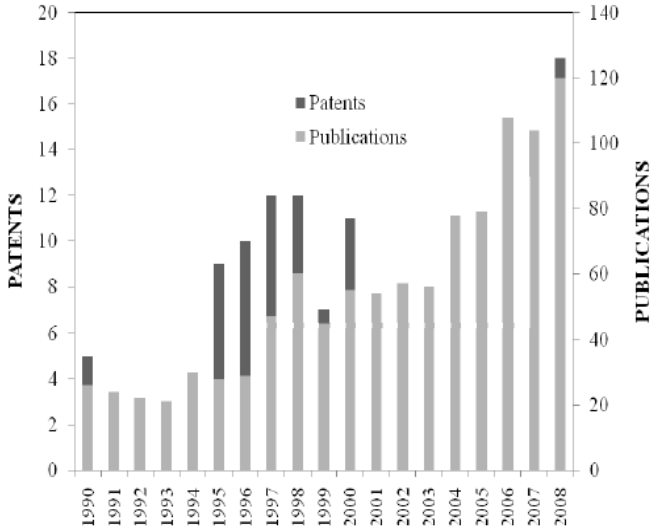

Figure 1.1 – Number of scientific publications and patents related to bacterial cellulose between 1990 and 2008 (Andrade *et al.*, 2010).

Biosynthesis of bacterial cellulose

The biosynthesis of cellulose on *G. xylinus* occurs between the outer and cytoplasmic membranes through the activity of a cellulose-synthesizing enzyme complex whose central enzyme is cellulose synthase. This complex is associated with the bacteria's outer membrane pores, whereby the bacterial cellulose is secreted (**Figure 1.2A**).

The enzyme cellulose synthase catalyses the last reaction of the cellulose biosynthetic pathway (**Figure 1.2A**), including the formation of cellulose from Uridine diphosphate-Glucose (UDP-Glucose). This enzyme has UDP-glucose as sole substrate

and, after its activation by cyclic diguanylate (c-di-GMP), chains of β(1→4) linked glucan (cellulose) are obtained as well as UDP as a by-product. (Jonas and Farah, 1998; Mayer *et al.*, 1991) The newly synthesized β (1→4) glucan chains abandon the cell membrane through its pores as microfibrils and are deposited outside the cell, assembling in 40-60 nm wide and 3-4 nm thick membranes by the bacteria (Andrade *et al.*, 2010), as it can be observed in **Figure 1.2A,** above. After the polymerization process was complete, the crystallization process follows, being this an autonomous process (Jonas and Farah, 1998; Mayer *et al.*, 1991). **Figure 1.2B**, by its turn, displays a micrograph of *G.xylinus* and synthesized BC nanofibres.

Culture conditions *Gluconacetobacter xylinus*

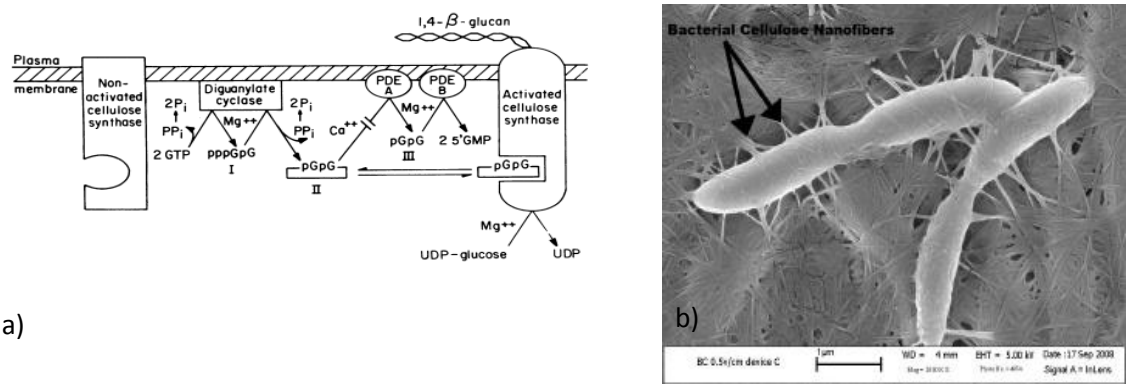

Figure 1.2 – A: Schematic representation of the bacterial cellulose synthetic pathway. The microfibrils are secreted through the outer membrane's pores assembler in layers thus forming a cellulose film of variable thickness on the extra-cellular space. **B: SEM micrograph of *G. xylinus.***

This species can be cultivated either in static or in stirred culture, with several variants for each culture method (Andrade *et al.*, 2010; Hornung *et al.*, 2007; Zuo *et al.*, 2006). The culture medium that is typically used to grow the bacteria was described by Hestrin and Schramm 1954 (Schramm and Hestrin, 1954) and is composed of glucose, yeast extract and bactopeptone and typically has a pH of 6.0. (Schramm and Hestrin, 1954). It can also be enhanced with other additives such as corn steep liqueur, molasses, among others, which grant higher biomass yields. The optimum growth temperature for *G. xylinus* is 30 º C, although high bacterial growth also occurs between 25 and 30 º C. The availability of oxygen is central to the growth of these bacteria as they are obligate aerobes (Andrade *et al.*, 2010; Schramm and Hestrin, 1954).

Static culture versus Stirred culture

Culturing *G. xylinus* in static culture is a relatively slower process and the produce BC is obtained in the form of a film with the shape of the fermentation vessel/reactor (**Figure 1.3A**) on the air-culture medium interface. The extraction process is very simple as it consists on the removal of the BC film directly from the reactor (**Figure 1.3A**) (Andrade *et al.*, 2010).

Culturing *G. xylinus* under stirring conditions, by its turn, yields both faster cell growth and cellulose production (Andrade *et al.*, 2010). However, less cellulose is obtained due to the spontaneous formation of cellulose-negative (cel^-) mutants which don't secrete cellulose under these conditions, thus only biomass being obtained (Valla, 1982). Also, the cellulose is produced in the form of small spheres (flocculated form) (**Figure 2.4B**), being this one of the main differences between static and stirred cultured (Cheng *et al.*, 2002).

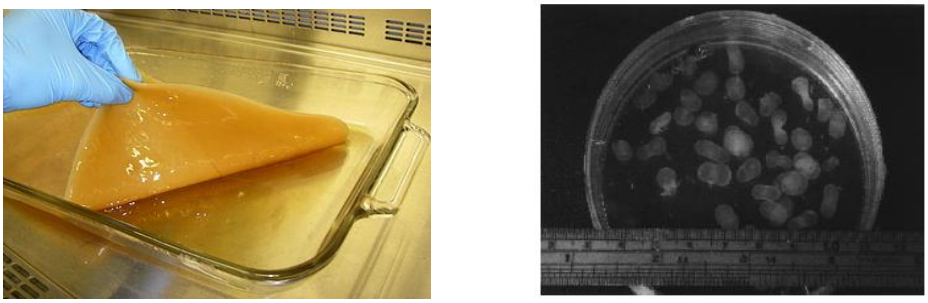

Figure 1.3 – A: Bacterial cellulose film collected after a static culture batch; B: Bacterial cellulose on its flocculated form, obtained after an agitated culture (airlift reactor) batch (Cheng *et al.*, 2002).

Factors that influence the production of bacterial cellulose

In addition to temperature and pH, the carbon and nitrogen sources as well as the bioreactor area and the used *G. xylinus* strain are highly impactful towards the BC yield and properties. This is especially important at the industrial level, where the carbon sources need to be more carefully chosen given the necessity of cheaper substrates in order to maximize the profit of the process.

Regarding pH, as mentioned earlier, the optimum value for the production of BC is 6 although a pH in a range between 4 and 7 is still acceptable (Masaoka *et al.*, 1992). Relatively to temperature, the optimal values are considered in between 25 º C and 30 º C (Schramm and Hestrin, 1954).

Properties

The general properties of bacterial cellulose are presented in **Table 1.2**. It is noteworthy that a change to the represented mechanical properties is observable after the exposure of the BC to high temperatures and/or pressures, being a change to its tensile strength and elongation registered (Iguchi *et al.*, 1988). The presented break strain values were measured using a 0.12 mm thick film (Sanchavanakit, 2006).

Table 1.2 – List of bacterial cellulose's properties (Andrade *et al.*, 2010).

BC Properties			
Morphological	**Water composition**	99%	
	Deg. of crystallinity	60-90%	
	Deg. of polymerization	2000-3000	
	Superficial area	12.6 m^2/g	
	Pore size	4.5-60 nm	
Mechanical	**Young's modulus**	16.9 GPa	
	Tensile strength	256 MPa	
	Elongation	1,70%	
	Break strain	**Heat dried film**	3.75%
		Wet film	8%
Others	**Water holding capacity**	**Hydrated**	1000%
		Dried (25 ºC)	106-60%
		Freeze dried	629%
	Porosity	**Dried (25 ºC)**	0.1 µm
		Hydrated	0.2-1.0 µm
	Permeability	Micro-channels of variable size.	
	Diffusivity	The solute diffusivity varies and can be verified especially on the entropic and hydrodynamic exclusions where only some partition and adsorption cases are verified.	

Bacterial cellulose application potential

As mentioned early, a very high application potential is recognized for the BC as its properties allow for the development of wide range of applications in the most varied fields such as the food, paper, electronic and even biomedical industries existing, already, some BC-based applications already in the market (Andrade *et al.*, 2010).

Food industry

BC has been used in the food industry for centuries being the Nata de Coco (**Figure 1.4**), a typical dessert from the Philippines composed solely of bacterial cellulose parting from the fermentation of coconut water, the most known (Andrade *et al.*, 2010). This was truly the first BC application and, additionally, the reason why BC was discovered.

This large scale product, which reached a high popularity level in Asian countries like Indonesia, Japan and Taiwan. (Andrade *et al.*, 2010), revealed a high economic potential given its popularity and profitability of production due to low-cost substrates usage and possibility of sustained continuous production (Jonas and Farah, 1998; Lapuz *et al.*, 1967). It was the success of the Nata de Coco that attracted the attention of major Japanese companies, such as Nakamori Vinegar and Japan Key Technology Center, towards the BC and a mobilized funds towards Biopolymer Research Co., Ltd, a company dedicated to the study and optimization of large scale production of bacterial cellulose in order to expand their success and harness the economic potential of bacterial cellulose (US Congress, 1993).

Figure 1.4 – "Nata de coco" food product.

Some research groups also describe BC as an excellent food additive that can be used towards different additives such as thickeners and stabilizers (Okiyama *et al.*, 1993; Okiyama *et al.*, 1992).

In addition to its use as a consumable food product, this biomaterial may also be used as a constituent of the packaging. Its effectiveness towards food preservation has already been demonstrated by Nguyen *et al.* in 2008, where positive results were obtained in the control of *Listeria monocytogenes*, a dangerous foodborne pathogen (Nguyen, 2008).

Paper industry

In an era where consequences of global warming are increasingly present, the search for alternative and eco-friendly materials for paper production has been increasing in order to avoid the over-exploitation of forest resources and promote their preservation.

Bacterial cellulose stands out as a very attractive choice as a substitute for vegetable cellulose given its physicochemical similarity to plant cellulose (Surma-Slusarska *et al.*, 2008) as well as being economically more attractive as no expensive and work-intensive pre-treatment and purification is required when compared to lignocellolusic biomass. Several authors have also described the applicability of bacterial cellulose in the process of paper recycling having already some paper recycling systems that use BC in the process are already beeng tested (Mormino and Bungay, 2003; Gostomski *et al.*, 2002).

Audio industry

As mentioned earlier in this chapter, bacterial cellulose can also be used as a constituent of audio systems existing, already, some successful commercial cases of products with cellulose on their assembly. This biopolymer displays both excellent dielectric and acoustic properties and, when conjugated with gold electrodes, exhibits good transduction over a wide range of frequencies (Markiewics *et al.*, 2004). These acoustic properties have a high impact on this sort of equipment, being strongly related to the acoustics, shape, strength and durability of the audio systems' speaker

diaphragms (Iguchi *et al.*, 2000; Indrartil *et al.*, 1998). All these features make this biomaterial a promising candidate in the production of high quality and high fidelity sound systems, being Sony the first company to produce and retail, in 1989, products built with bacterial cellulose membranes on its assembly.

Biomedical applications

The high biocompatibility and durability of BC provided the development of biomedical applications in regenerative medicine, tissue engineering, and wound treatment, among others. The interactions between cells and BC have been studied, being the bacterial cellulose considered a good mammalian cell substrate (Watanabe *et al.*, 1993). In addition, modifications were made to the BC such as the conjugation with adhesins in order to further improve its interaction with cells that lack the anchoring support.

Relatively to cytoxicity/biocompatibility, these were assessed by evaluating in vitro the viability and proliferation of skin cells and in vivo by introducing subcutaneously a nanocellulose membrane on mice (Sanchavanakit *et al.*, 2006; Helenius *et al.*, 2006). It was found that bacterial cellulose displayed no cytotoxicity and the growth of skin cells was normal *in vitro*. As for the *in vivo* tests, the organism also displayed good acceptance towards the BC since no adverse reaction was verified and the body's cells infiltrated the cellulose's fibrous network and vascularization of the implant's area (Andrade *et al.*, 2009; Pértile *et al.*, 2007) was verified.

Regenerative medicine and tissue engineering

At the level of regenerative medicine and tissue engineering first advances have already been made regarding the use of BC and there are already a few commercial applications in the market. Some examples of these applications are Gengiflex (Novaes *et al.*, 1993), Biofill (Fontana *et al.*, 1990), Bioprocess and BASYC (Bacterial synthesized cellulose) (Klemm *et al.*, 2001).

When it comes to tissue engineering, BC has also been tested has a base material for the development of artificial blood vessels and dental implants (Backdahl *et al.*, 2006; Anjos *et al.*, 1998). From the previously stated examples, however, the artificial blood

vessels display the most importance since cardiovascular diseases are the main cause of disability or death according to World Health Organization (WHO)'s data. The main challenge inherent to the development of artificial blood vessels lie on the necessary modifications in order to promote the adhesion of endothelial cells to the implant as well as possible rejections by the body (Anjos *et al.*, 1998). However, despite these challenges, several authors demonstrated positive results in the application of BC in the construction of artificial blood vessels achieving not only a good acceptance by the organism but also the tissue's endothelization and survival of the animals on which tests were made (Anjos *et al.*, 1998).

Intrinsically Conducting Polymers (ICP)

During the initial years of their discovery, polymers were regarded as good electricity insulators. However some research groups began to discover and describe the occurrence of polymers endowed with electrical conductivity. The major paradigm-shifting breakthrough happened in 1978 when Shirakawa *et al.* demonstrated that polyacetylene, an electrically insulating polymer, displayed an abrupt increase on its electrical conductivity when processed with an oxidizing or a reducing agent (Chiang *et al.*, 1978; Chiang *et al.*, 1977).

This re-discovery of polyacetylene as an intrinsically conductive polymer (ICP) triggered an intensive and multidisciplinary research activity directed towards the discovery and characterization of new ICP systems (Aldissi, 1984). As a result of this research activity throughout the years, many new ICPs have been discovered and described; these include polyfuran, polyaniline, polyisothianaphtene and polypyrrole (PPy), to name a few.

Regarding electrical properties, as already mentioned above, while these polymers display an almost null conductivity in their native state, their electrical conductivity is highly increased through oxidation/reduction, or doping, which occurs during their synthesis. The electrical conductivities of these polymers are in the range of 10^{-12}-10^{6} $S.cm^{-1}$, taking their uncharged state in account, being these polymers mostly semi-conductors except for some cases (e.g. doped polyaniline and poliacetilene)

(MacDiarmid, 2001). **Figure 1.5** displays the range of electrical conductivity of several materials, so that the classification of the ICPs can be more clearly understood.

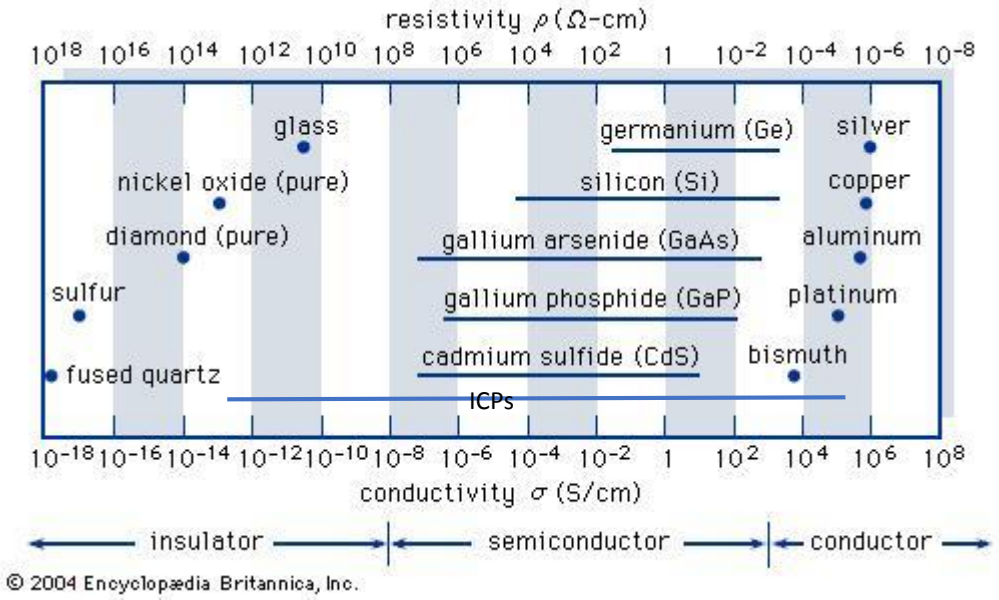

Figure 1.5 – Range of conductivity for insulator, semiconductor and conductor materials (Encyclopaedia Britannica, 2004).

One inherent property to some of these polymers is their toxicity, however, there are some cases where this isn't verified being PPy an example of a conductive polymer that is considered biocompatible, as it displays low cytotoxicity at low concentrations (Vaitkuviene, 2013)). These polymers also have poor processability as they're usually obtained in mechanically feeble films or intractable powders which may be limiting towards their usage on application development.

Synthesis

The synthesis of ICPs can be made either chemical or electrochemically (Saville, 2005). The electrochemical synthesis consists of the exposure of a monomer solution to an electrode which will promote the polymerization process by either oxidizing or reducing the monomers being the synthesized polymer deposited under the form of a thin layer on the electrode's surface.

The chemical synthesis method, on the other hand, consists of the previous doping of the monomers by partial oxidation (p-doping) or reduction (n-doping) followed by the polymerization reaction. The doping process consists of the modification of the

monomers' intrinsic nature by inserting a different chemical specie (dopant) onto their structure thus altering its electrical properties. As mentioned above, this process can occur either by oxidizing the monomer with an oxidizing agent or reducing it with a reducing agent.

When the monomer is oxidized, or p-doped, it will lose an electron for the oxidizing agent (*e.g.* ferric chloride ($FeCl_3$)), hence forming a radical cation (**1**). Alongside this reaction, a counter anion, usually prevenient from the oxidizing agent (*e.g.* Cl^- from $FeCl_3$) is also inserted in the monomer's electron cloud thus forming an electrically neutral complex. However, despite the electrical neutrality of the complex, the existence of regions within' the compounds' lattice that are positively charged due to oxidation and negatively charged due to the presence of the counter anion promote charge delocalization throughout the entirety of the polymer's structure due to electron transfers which, in turn, lead to the electrical conductivity of the ICPs (McDiarmid *et al.*, 1985).

The n-doping process, by its turn, is equal to the p-doping process but a reducing agent (*e.g.* ascorbic acid) is used and the formation of a radical anion (**2**) occurs instead. Regarding the necessary counter ion, for the n-doping case, a counter cation is necessary in order to create the electrically neutral complex.

$$\mathbf{Polymer} + \mathbf{X} \leftrightarrow (\mathbf{Polymer})^{\mathbf{n+}} + \mathbf{X}^{\mathbf{n-}} \quad \textbf{(1)}$$

$$\mathbf{Polymer} + \mathbf{M} \leftrightarrow (\mathbf{Polymer})^{\mathbf{n-}} + \mathbf{M}^{\mathbf{n+}} \quad \textbf{(2)}$$

In short, it is the doping process that leads to the formation of a charged polymer as, otherwise, the polymer would be obtained in its neutral state hence being an electrical insulator.

It is noteworthy that the doping level, concentration of dopant present in the compound's structure, is highly impactful towards the electrical conductivity (Saville, 2005).

The solvent in which the polymerization reaction occurs is also impactful to the polymer's final mechanical and electrical properties. For example, in the PPy synthesis, the loss of a proton by the pyrrole (Py) monomers during the polymerization process

occurs hence solvents which are good proton acceptors, such as water, will enhance the polymerization process.

(Poly)pyrrole

Polypyrrole was one of the first ICPs to be electrochemically synthesized. This was achieved by Dall'Olio in 1968 who obtained, using a platinum electrode and sulphuric acid (H_2SO_4), a powdery precipitate that was denominated "pyrrole black" (Linford, 1990).

Polypyrrole Structure

The PPy ($[C_4H_5N]_x$) structure consists of Py (C_4H_5N) monomer units (**Figure 1.6A**) coupled through their 2- and 5- positions (**Figure 1.6B**). (Saville, 2005; Linford, 1990)

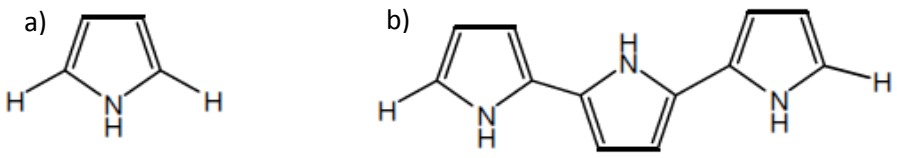

Figure 1.6 – A: Pyrrole monomer; B: Three pyrrole units coupled through their 2- and 5- positions (Saville, 2005).

This ICP displays four distinct forms, two in the neutral state, the aromatic (**Figure 1.7A)** and quinoid forms (and **1.7B**), and two related in the oxidized state, the polaron and bipolaron, depending on the number of positive charges present in the polymer's backbone (**Figure 1.7C**) and/or a bipolaron (**Figure 1.7D**) (Saville, 2005).

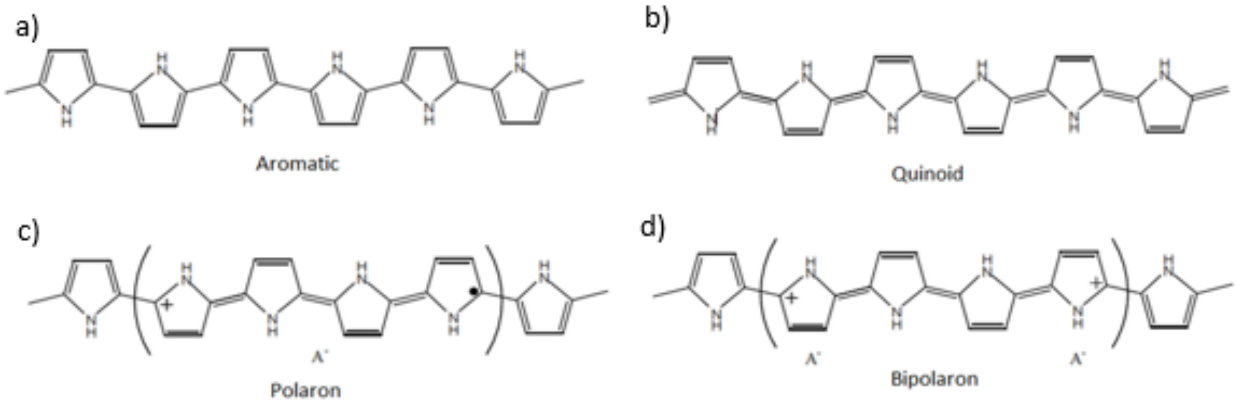

Figure 1.7 – The four forms of polypyrrole. A: Aromatic (neutral); B: Quinoid (neutral); C: Polaron (charged); D: Bipolaron (charged) (Saville, 2005).

Polypyrrole chemical synthesis

Despite the existence of two methods for pyrrole synthesis, electrochemical and chemical polymerization, only the chemical synthesis process will be explained in detail as it was used in this work.

Overall, the PPy synthesis can be summed up to of a 4-step process:

Step 1.

The Py monomers are p-doped by using an oxidizing agent. $FeCl_3$ is the most commonly used as it yields higher electrical conductivities (Machida and Miyata, 1989); the oxidation is thus mediated by $Fe3^+$, being Cl^- the counter-anion.

Step 2.

Two radical cations are combined through the formation of a linkage between the second position of the pyrrole ring (2-2 linkage), forming 2,2'-bipyrrole, which is followed by the loss of two protons (H+).

Step 3.

The previously formed bipyrrole dimers are further oxidized and combined, similarly to what happens in **Step 2**, thus forming an oligomer.

Step 4.

The final step of the reaction occurs when there are no more pyrrole monomers present for the polymerization reaction. Some side reactions can, however, also terminate the PPY chain thus ending the polymerization process.

Figure 1.8 illustrates the first three steps of the PPy polymerization. **Step 4** is not displayed as it corresponds to the polymerization's terminus which corresponds to a PPy chain and no more monomers are added (**Step 2**).

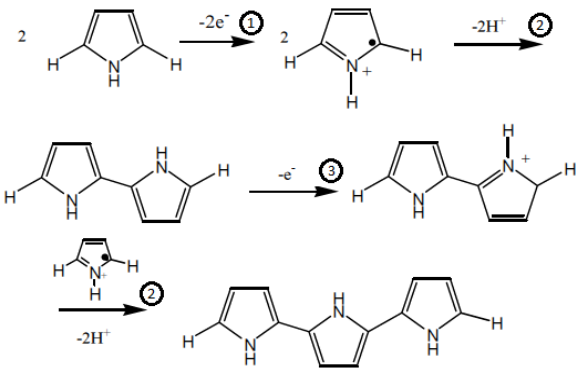

Figure 1.8 – The polypyrrole polymerization reaction. (Saville, 2005)

AS observed above, the conductivity of the resulting PPy film is strongly influenced by the redox potential of the ferric cation (Fe2+/Fe3+) which, by its turn, is influenced by the acid anions (*e.g.* Cl^-) and solvent used. The redox potential of the ferric cations may be reduced by adding weaker acids, which coordinate them more strongly.

Regarding the solvent, as mentioned above, it also plays an important role toward the regulation of the redox potential of the ferric cations and, consequently, electrical conductivity. Among the solvents used for PPy synthesis, water is the one which yields PPy with the highest electrical conductivity (Saville, 2005). This is due to the fact the redox potential of the ferric cations in water is the lowest compared to other solvents as water is a protic polar solvent with the highest dielectric constant, which means that the ferric cations will be strongly coordinated by the water molecules by solvation. In short, the choice of the solvent is very impactful towards the obtained polymer as it can be the difference between electrical conductivities of 3 $S.cm^{-1}$ and 500 $S.cm^{-1}$ as well was more or less processability as **Table 2.3** illustrates.

Table 1.3 - Solvent's impact on the PPy electrical and mechanical properties.

Solvent	Ratio (%)	Maximum conductivity (σ) ($S.cm^{-1}$)	Tensile strength (Psi)	Elongation (%)
Acetonitrile/Water	99:1	100	8,600	4
	99:1	30	6,200	17
	75:25	0.5	2,700	6
Ethylene Glycol/Water	50:50	17	2,700	6
Acetonitrile/Ethylene Glycol	75:25	25	4,750	5
	50:50	29	7,210	8
Acetonitrile/Ethylene glycol/Water	50:25:25	3	5,310	6
Water	100	500	_____	_____

Comparatively to electrochemically synthesised PPy, chemically synthesized PPy is identical to its counterpart in terms of composition and electrical conductivity (Ansari, 2006; Saville, 2005). The major difference is that chemically synthesized PPy's processability is much lower than electrochemically synthesized PPy as it is obtained as an intractable powder (Saville, 2005). However, the usage of chemically synthesised PPy is attractive towards the synthesis of hybrid conductive composites composed PPy and other materials which can be used as insulation matrices as PPy can be polymerized *in situ* on the material's matrix (Ansari, 2006). A good example of materials that can be used as insulator matrices are fibrous such as viscose and polyester (Dall'Acqua, 2006; Macasaquit and Binag, 2010) or bacterial cellulose as it was accomplished in this work and will be described below.

Application potential of intrinsically conductive polymers

The ICP family's members can be used majorly on the development of capacitors and solid state batteries of high Coulombic efficiency due to their excellent electrical properties and the ability to store high amounts of energy. Additionally, due to their low mass and the possibility of being synthesized under the form of thin films allows the construction of light-weight, thin and highly efficient batteries. Among the vast family of ICPs, PPy is the one that displays the highest potential towards the development of this type of applications due to its facile and cost-effective synthesis, environmental stability and high electrical conductivity (Vernitskaya and Efimov, 1997).

Another potential application of PPy is in sensors and actuators (Vaitkuviene *et al.*, 2013; Jin *et al.*, 2000; Vernitskaya and Efimov, 1997), due to some interactions that different that chemical agents can have on the ICPs' electrical conductivity (*e.g.* films of polyaniline have different colors depending on the pH), these polymers can be integrate various types of sensors such as gas and pH sensors (Vernitskaya and Efimov, 1997; Jin *et al.*, 2000). Moreover, as some of these polymers are biocompatible, they can even be integrated on biosensors such as catalytic biosensors and imunosensors (Vaitkuviene *et al.*, 2013).

Some ICPs (*e.g.* Polyvinylidene fluoride) also display piezoelectric properties, which means that they accumulate electrical charge in response to applied mechanical stress, which opens up the possibility of implementation in the development of mechanical sensors and, to a certain degree, self-recharging batteries (Xue *et al.*, 2013; Wang *et al.*, 2011).

As for PPy, additionally to some of the aforementioned applications, it can also be integrated onto applications in the field tissue engineering, biosensors and drug delivery systems as it is cheap, easy to synthesize, stable and biocompatible (Vaitkuviene *et al.*, 2013). It can also be incorporated onto other material's matrices, in order to form hybrid electrically conductive composites that display both the host material as well the polymer's properties. One material that can be used as an insulation matrix for PPy and posteriorly used in the development of these composites is BC, being this specific case detailed in the section below as it is the main focus of this work.

PPy and BC (BC-PPy) conductive composites

As already mentioned earlier, it is possible to conjugate ICPs and BC by using it as an insulation matrix for these polymers in order to obtain electrically conductive BC-ICP composites. Among the plethora of the existing ICPs, PPy is one of the most suitable member of this family for this purpose due to not only its good electrical properties but also due to the simplicity of its synthesis process as well as its biocompatibility and stability (Al-Mashat *et al.*, 2008; Babu *et al.*, 2012).

The BC-PPy composites can be obtained by incorporating PPy on the BC matrix through *in situ* polymerization, being the polymerization often in aqueous solution (wet chemical polymerization (WCP)). This *in situ* synthesis method is similar to the chemical PPy synthesis, however, it occurs directly on the surface of the BC nanofibers. The synthesis process consists of the oxidation of the BC using an oxidizing agent thus occurring the *in situ* p-doping of the Py monomers, mediated by the dopant present in the fibres. The BC oxidation step is performed by dipping the material into an aqueous solution of the oxidizing agent. Posteriorly, the oxidized material is immersed on a Py monomer solution of known concentration thus triggering the polymerization reaction being a PPy layer formed around the material's fibres (Beneventi *et al.*, 2006).

Additionally to the WCP, another method of synthesis has been thought of as viable hence being an adaptation of this method implemented towards the synthesis of BC-PPy. This method, designated as chemical vapour deposition (CVD), was described by Dall'Acqua in 2006 as a simple, inexpensive and free of solvents process. The synthesis of composites using the CVD method consists of the oxidation of the material using an oxidant and its posterior exposure to Py vapours. (Dall'Aqua *et al*., 2006). The main advantage of this method, aside from its simplicity, resides in the fact that the excess of unpolymerized Py in the end of the process is recyclable (Dall'Acqua *et al.*, 2006).

Potential Applications of BC-PPY composites

The development of these electronically conductive BC-PPy composites opens up a place for BC-based applications on the electronics industry. These composites can be used to develop various types of applications such as displays, OLED's (Organic Light-

Emitting Diodes), transistors and conductive membranes (Andrade *et al.*, 2010; Legnani *et al.*, 2008; Shah *et al.*, 2005). Additionally, the electronics industry, similarly to the paper industry, is beginning to suffer from the stigma of resource over-exploitation, more specifically the depletion of materials that are incorporated in electronic devices being depletion of Indium, a rare metal with excellent conductive properties that is widely used as the main component of the displays, luminescent panels, photovoltaic cells, among others, one of the main issues. As such, the discovery of new materials that can be used in the production of these electronic devices is increasingly necessary.

Flexible electronic materials

The most interesting application potential that the use of BC may bring to electronics is the development of flexible electronically conductive materials that are also lightweight, biodegradable and highly recyclable (Shah *et al.*, 2005).

Electronic Paper, e-papers, e-books, displays and flexible tablet PCs are idealized concepts being some of them already prototyped undergoing tests (Shah *et al.*, 2005). Some already conceived examples of these innovative applications are PaperTabs, under development by Intel, Plastic Logic and Queen's University, and the Samsung OLED whose technical concepts revolve around flexible electronic tablet PCs and were presented by their respective developers on the 2013 edition of the International Consumers Electronics Show (International CES) promoted by the Consumers Electronics Association (CEA).

Biomedical electronics

The possibility to use BC as an OLED brings potential utility to the medical field since it could allow its incorporation onto flexible displays for therapeutic purposes such as photodynamic therapy, targeting the treatment of skin cancer and other diseases (Nogi *et al.*, 2006; Yano *et al.*, 2005).

Some other examples of possible applications of electrically conductive BC-PPy composites in this field are also biosensors such as temperature sensors which may be incorporated in probes or catheters hence providing accurate information about tissue temperature variations (Nambiar and Yeow, 2011; Bagavathiapan *et al.*, 2008).

The integration of micro-electromechanical system-based sensors on BC-PPy membranes is also a possibility that could open a window of opportunity towards the design of very sensitive and specific surgical tools which, in conjunction with flexible display systems, would provide significantly easier and least invasive surgical interventions as smaller incisions would be necessary (Nambiar and Yeow, 2011). These improvements are very beneficial for both the surgeons and especially the patients as the reduction of blood loss, risk of infection and a quicker recovery are the main advantages that these changes would bring (Schostek *et al.*, 2009).

Another promising application of BC-PPy membranes is their potential use as a cell growth-stimulating support being already some experiments with similar composites reported in the literature (Bidez III *et al.*, 2006; MaCdiarmid, 2001). It is, however, noteworthy that on the development of this type of applications the oxidizing agent must be carefully chosen as cytotoxic oxidants such as $FeCl_3$ would lead to cell death.

Chapter 2. Materials and Methods

In this chapter a description of the various experimental procedures used throughout this work will be made starting by a detailed explanation of the theoretical concepts of each technique followed by a section where the experimental conditions are presented and described.

Theoretical Concepts

Electrical conductivity measurements

In order to determine the electrical conductivity of the BC-PPy membranes their resistivity was firstly determined. The electrical resistivity (ρ) is the measurement of a material's resistance to an electric current across its volume hence it is expressed in Ohm meter (Ω.m). The ρ was calculated according to **Equation 2.1** being the cross section of the samples considered uniform:

$$\rho = R\frac{A}{l} \qquad \textbf{(2.1)}$$

where R, A and l are the electrical resistance (Ω) of the sample, A is the area of the analysed cross-section and l is the thickness of the sample, respectively.

The electrical conductivity (σ), by its turn, is the inverse of the electrical resistivity, namely, a material's ability to allow the passage of an electric current ($\sigma = \rho^{-1}$), expressed in Siemens per meter ($S = \Omega^{-1}$).

The electrical resistivity of the BC-PPY membranes was then determined using two different methods: two-point measurement and four-point measurement using a four-point collinear probe. On both methods an electrical current with variable voltage or intensity, depending on the used method, is applied to the sample. On the two-point measurement technique the applied current has variable voltage within a specified range while on the four-point measurement technique it has variable intensity within a specified range.

A brief explanation of both techniques is given below, separately.

Two-point measurement technique

For the two-point measurement technique, two probes are used, one for the applied electrical current and another for the measurement of the intensity of the conducted current.

Posteriorly to the measurements of the current's intensity and an IV (Intensity vs Voltage) curve is obtained by plotting the voltage and intensity values on the abscissas and ordinates axes respectively. The electrical resistance (R), which is necessary to determine the sample's resistivity through **Equation 2.1**, is then obtained through the linear regression of the IV curve thus corresponding to the slope of the obtained trend-line accordingly to the Ohm's law (**Equation 2.2**):

$$R = \frac{V}{I} \qquad \textbf{(2.2)}$$

Finally, the resistivity of the material is determined through **Equation 2.1** by using the sample's electrical resistance and thickness (l / m) and the conductivity value is then obtained by using $\sigma = \frac{1}{\rho}$.

For the two-point measurement technique a Keithley 487 Picoammeter/Voltage Source (circuit shown in **Figure 2.1**) was used. The measurements were made with the sample within a Faraday cage in order to diminish possible interference of surrounding electrical fields as well as mechanical vibrations on measurements.

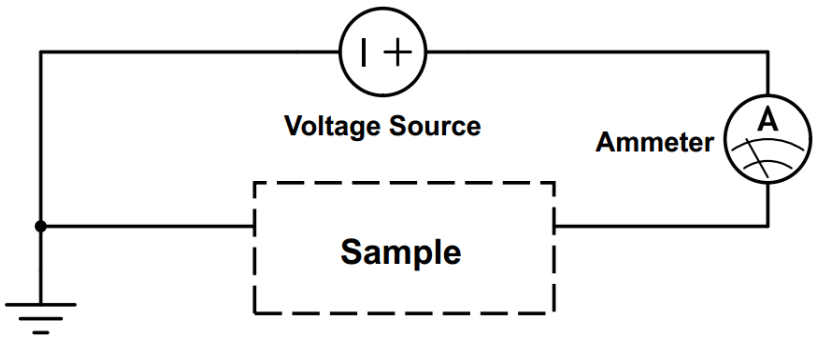

Figure 2.1 – Circuit used in the two-point measurement technique.

Four-point collinear probe resistivity measures

Given that BC-PPY membranes synthesized by WCP displayed very high conductivity comparatively to the ones obtained by CVD (semi-conductor class conductivity) it was necessary to use a measurement method with a higher resolution. Indeed the two-point measurement method could only allow a reliable resistivity measurement within a range of values of up to the 10^{th} order of magnitude of the Ω.m (10 GΩ.m). The selected method for the conductivity assessment of the BC-PPy membranes was, as stated above, the four-point collinear probe which, in turn, has a much higher resolution as it is used for the determination of semi-conductors resistivities in the range of the nΩ.m as well as lower error measurements (i.e. higher sensitivity).

The method for the determination of the electrical resistivity and conductivity was similar to the above: an IV curve was obtained posteriorly to the measurements and the electrical resistance was obtained through a linear regression. The resistivity was then calculated using (**Equation 2.3**):

$$\rho = \frac{2\pi SV}{I} \qquad \textbf{(2.3)}$$

where, S is the probe spacing (mm; constant), I is the supplied current, and V the measured voltage. Conductivity was then calculated using $\sigma = 1/\rho$.

The electrical measurements were made using a Time Electronics 9818 DC Current Voltage Calibrator current source and the electrical potential difference was measured using a Keithley 2182 Nanovoltmeter - **Figure 2.2** shows the circuit scheme.

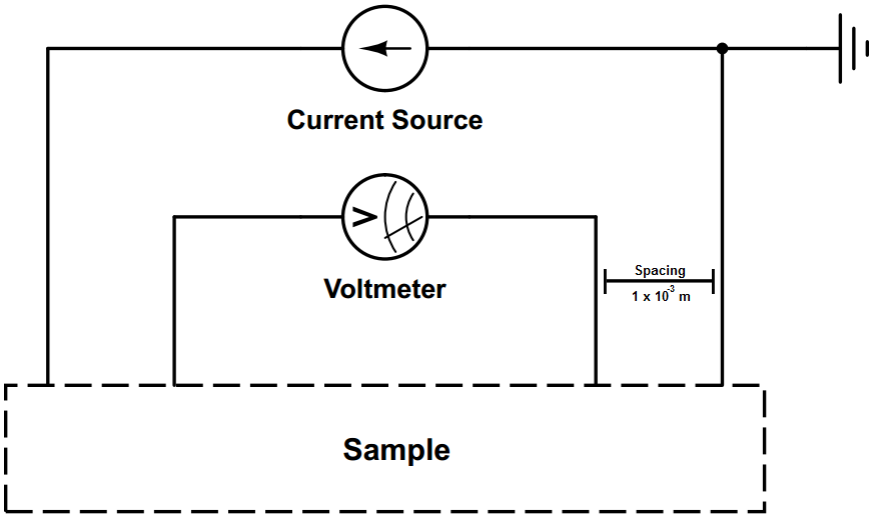

Figure 2.2 – Circuit used in the four-point collinear probe measurement technique. The outward probes (1,2) are sourcing the current while the inward probes (3,4) measure the electrical potential difference across the sample's surface. All the probes have an equal spacing between them – as shown in the scheme.

Mechanical Characterization

For the mechanical characterization of the BC-PPy membranes tensile strength tests were performed.

The universal testing machine (**Figure 2.3**) is generally composed of a load frame which serves as the machine's support; a load cell for measuring the load; two cross heads, in the case of the performed tests, where the sample is griped, the cross heads move in opposite directions thus applying strain to the samples; an extension/deformation measurer in order to measure the response of the sample to the applied strain; and an output device which records the assay's data namely the temperature, elapsed time, applied force in Newtons (N), distance between the cross heads in meters (m), the mechanical stress in Pascals (Pa) and the strain/elongation.

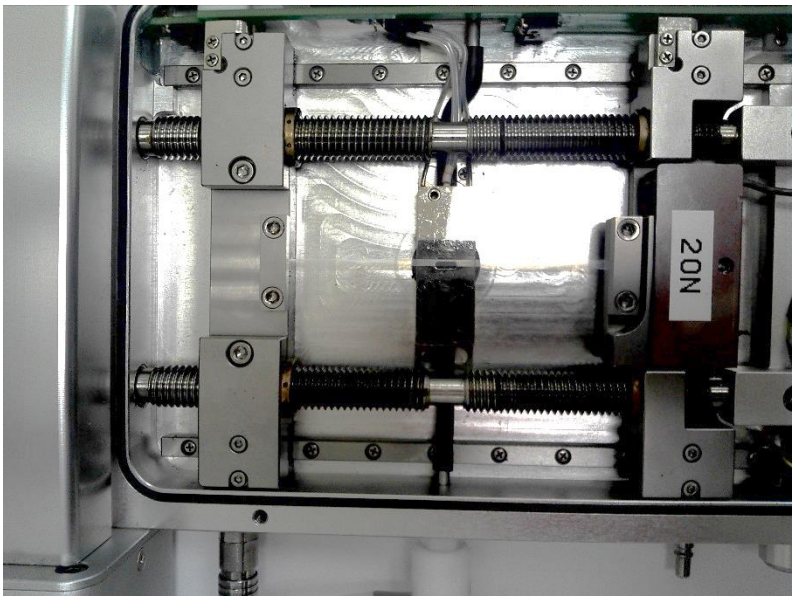

Figure 2.3 – Linkam TST350 Universal Test Machine. Highlighted: Cross-heads to which the sample is griped.

Data analysis

Parting from the acquired data after the tensile testing, the ultimate tensile strength (UTS) and the Young's modulus were determined. The UTS is easily determined as it corresponds to the strain value measured right before the sample breakage – when the measured stress value starts to diminish).

The Young's modulus (E), by its turn, is determined according to the following equation (**Equation 2.4**):

$$E = \frac{\sigma}{\varepsilon} \qquad \textbf{(2.4)}$$

where σ and ε correspond to the tensile stress and tensile strain, which, by their turn, correspond to the measured stress and strain values at the sample breakage.

The Young's modulus of the samples was then determined by plotting the mechanical stress values versus the strain values until the breakage point, which corresponding to the linear part of the stress-strain curve, and a linear regression was applied thus corresponding the slope of the obtained trend line to the material's Young's modulus value.

Scanning Electron Microscopy (SEM)

The Scanning Electron Microscopy (SEM) is an imaging technique introduced in 1933 by Ruska (McMullan, 1989); this powerful technique is widely used for the characterization of materials' surface topography as it allows the obtainment of 3D images of the sample's surface as well as its cross-section thus allowing for the study of its composition and study not only in surface but also in volume.

The SEM technique consists of the irradiation of the analysed sample with an electron beam with variable energy ranging between 200 and 4 x 10^4 eV which scans the sample; the energy of the electron beam is chosen according to the characteristics of the analysed sample.

The electrons interact with the sample, which is previously coated with a conductive substance (e.g. gold) through sputtering, thus losing energy given to scattering and absorption within the chosen field of view which can vary according to the selected magnification. The image is generated through the detection of the beam current variation across the sample and its posterior synchronization with a computer video memory which, by its turn, generates the image which is equivalent to the distribution map of the signal intensity across the analysed section of the sample.

The instrument used for this technique is the scanning electron microscope (**Figure 2.4**) which is composed by: the electron beam gun, two condenser lens that allow the focusing of the electron beam thus obtaining a beam with a small diameter, a conjunction of deflection coils which allow the scanning of the sample by deflecting the electron beam, a vacuum pump, an objective lens and an electron detector which allows the image obtainment.

The equipment used for the SEM analysis of the samples was a Leica/Cambridge S-360 SEM.

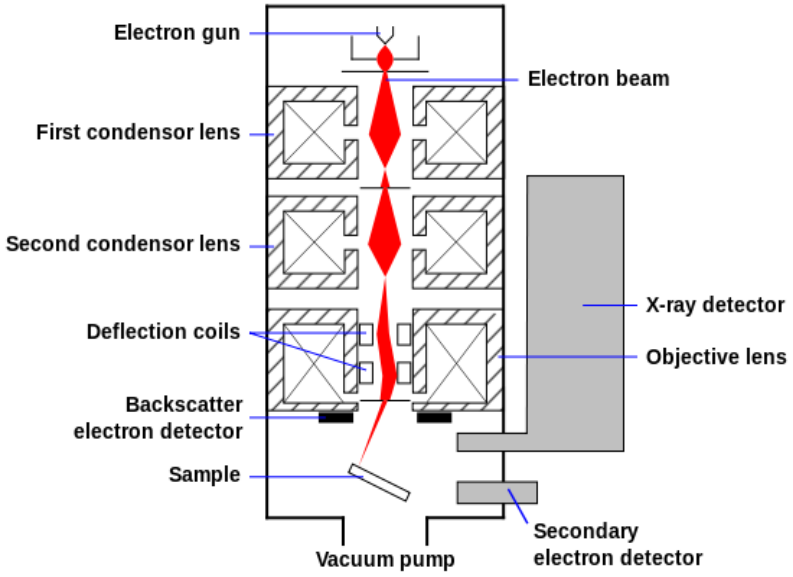

Figure 2.4 – Representation of the SEM microscope and its respective components.

Fourier Transform Infrared Spectroscopy by Attenuated Total Reflectance (FTIR-ATR)

The Fourier transform infrared spectroscopy (FTIR) is spectroscopic technique that is widely used for the characterization, identification (fingerprinting) and/or quantification of materials. The most appealing aspect that this technique brings is the fact that it allows the analysis of samples on their solid, liquid or even gaseous states. The analysis through the FTIR technique consists of the transmission of a variable wave-length radiation in the infra-red region through the sample thus obtaining an infra-red absorption spectrum. This occurs due to the fact that when the material's molecules equilibrium is disturbed by the incidence of the IR beam they will vibrate with a given frequency that, when in the infrared (IR) region, causes the molecule to absorb radiation which enables the determination of specific components and/or chemical groups that absorb a specific IR frequency and posterior chemical determination of the sample (Barrios *et al.*, 2012).

Excluding some homonuclear molecules such as O_2, N_2 and Cl_2, all the molecules absorb radiation within the infra-red range and every molecule has a characteristic IR spectrum. The IR spectra are composed of absorption peaks on specific wavelengths

distributed throughout the spectrum hence why each molecule has a characteristic IR spectrum.

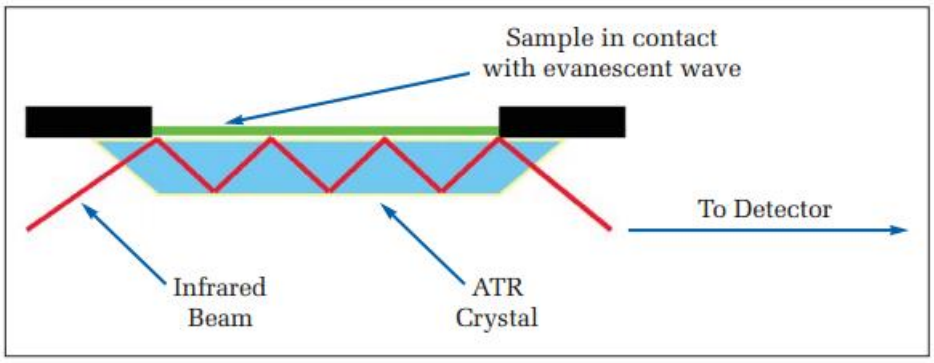

Figure 2.5 – Explanation of the ATR technique. The infrared beam passes through the ATR crystal with a 45 º (on the figure) angle of incidence and is reflected through the interior of the crystal hitting at least one point where the crystal is in contact with the sample. The IR beam is then collected by the IR spectrometer's detector which gives the IR spectrum.

The attenuated total reflectance (ATR) technique, by its turn, is a FTIR analysis that uses an optically dense crystal (ATR crystal) with a high index of refraction, pressed into contact with the sample (Barrios *et al.* 2012). The IR beam emitted by the IR spectrum passes through the crystal with an angle of incidence at which it is reflected through its interior. The internal reflectance of the light forms an evanescent wave which penetrates a few microns of the sample, depending on the light's λ, the angle of incidence and the index of refraction of the ATR crystal. The reflected IR beam is then finally passed to the detector on the IR spectrometer that, consequently, generates the IR spectrum. **Figure 2.5** above gives a schematic representation of the ATR technique.

The samples were analysed using a PerkinElmer Spectrum 100 FT-IR Spectrometer using the HATR sampling accessory also from PerkinElmer. The ATR crystal was a zinc selenide (ZnSe) crystal which has a refractive index of 2.62.

X-Ray Diffraction (XRD)

The x-ray diffraction, or XRD, is an analytical technique that is used for various purposes such as: determine the orientation of crystals or grains, identify the crystalline structure of a material as well as measuring the size and shape of small crystalline regions (Warren, 1969).

The XRD phenomenon, which consists of the x-ray reflection by the cleavage faces of crystals, is explained by the Bragg's law (Warren, 1969) (**Equation 2.5**):

$$n\lambda = 2d.\sin(\theta) \qquad \textbf{(2.5)}$$

where n, λ, d and θ are an integer, the wavelength of the incident x-ray beam, d is the distance between atomic layers in the crystal and the angle of incidence respectively.

The angle of incidence corresponds to the angle between the x-ray beam transmitted through the sample and the diffracted beam

The XRD technique consists of the incidence of a beam of x-rays on a crystal (sample) which, by its turn, will be diffracted given the interference between the rays by passing through the crystalline structure thus being diffracted by the atoms of its atomic lattice (**Figure 2.6A**). The XRD pattern is then recorded on a photographic film which, by its turn, displays an arranged pattern of: well-defined spots (**Figure 2.6B**) that correspond to the diffracted x-rays around the spot that corresponds to the central transmitted beam (single-crystal samples); intersecting rings around a central spot (**Figure 2.6C**) which corresponds to the transmitted beam (powder samples). The intensity of the spots varies according to the intensity of the beam and is determined by a detector coupled to the end of the system.

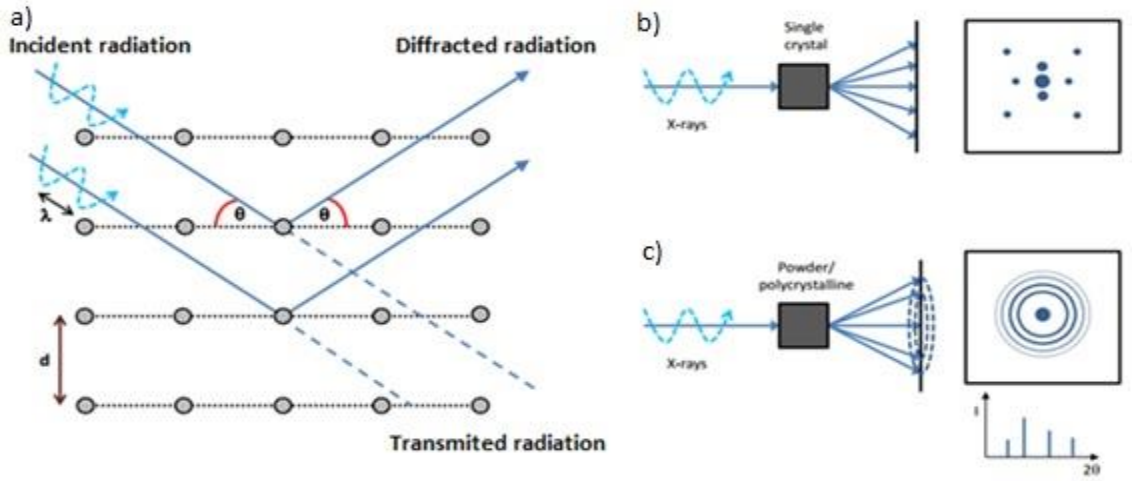

Figure 2.6 – A: Representation of the diffraction of the incident x-rays in the atomic lattice of the sample; B: XRD pattern obtained when analyzing a simple crystal sample; C: XRD pattern obtained when analyzing a powdery sample.

The piece of equipment which is used for the XRD analysis is the diffractometer (**Figure 2.7**) which is composed of an x-ray tube/gun, a sample holder and a detector.

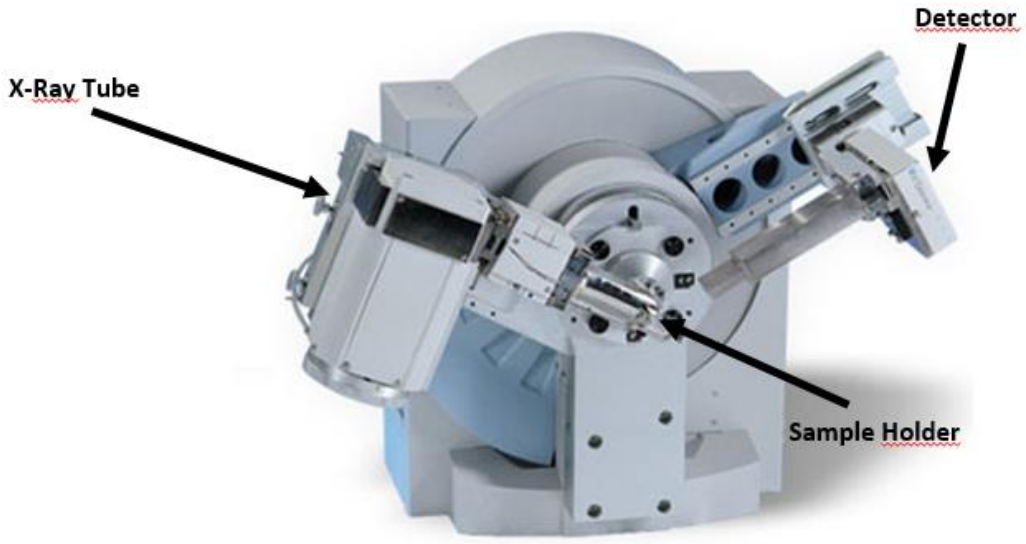

Figure 2.7 – X-Ray diffractometer and its components.

Analysis and interpretation of XRD patterns

The XRD pattern is then obtained in a graph that contains the diffraction angle (2θ) as the XX axis and the intensity of the diffracted beam as the XY axis.

The intensity peaks, or diffraction peaks, that are possible to observe on an XRD pattern correspond to the diffracted x-rays. Their intensity is determined by the electron density of the sample since, when a sample has a greater number of electrons, the x-rays will be suffer higher scattering thus generating peaks of greater intensity. The d spacing value is also a contributing factor for the intensity of the peaks and is more relevant when analysing powdery samples.

Through the analysis and interpretation of the peaks it is possible to assess the material's crystalline structure, by calculating the peaks' area, size of crystalline structures, by measuring the width of the peaks, as well as the d-spacing and lattice parameters according to the peaks' positioning.

The reason why this technique was chosen to characterize the BC-PPy membranes is because that, through comparison of the XRD pattern of the BC-PPy membranes and pure BC it is possible to assess if the modification of the BC fibres with the PPy affects the BC's crystalline structure. For the characterization of this material a Philips Analytical

X-Ray model PW 1710 BASED powder diffractometer with CuK_α monochromatic radiation at 40 kV, 30 mA and with a λ of 1.5406 Å was used and the analysed samples were pure BC, cBC-PPY, wBC-PPY and pure PPY powder.

Thermogravimetric Analysis (TGA)

The TGA technique is commonly used in order to study the aforementioned characteristics of materials among other physicochemical properties and phenomena such as: second-order phase transitions, water holding capacity, adsorption, etc. The analysis consists of the heating of the sample to a desired temperature (e.g. 800 ºC) with a controlled heating rate (β) while registering the sample's mass variation during the heating process (Coats and Redfern, 1963). Regarding the apparatus, the TG analyser (**Figure 2.8**) is composed of a precision quartz crystal microbalance (QCMB), a programmable furnace and a crucible where the loading of the samples is done.

Analysis interpretation of the thermal decomposition pattern

In order to study the thermal decomposition pattern of the samples, it is necessary to plot the sample's weight variation in percentage during the course of the analysis versus the temperature – thermogram or TGA curve.

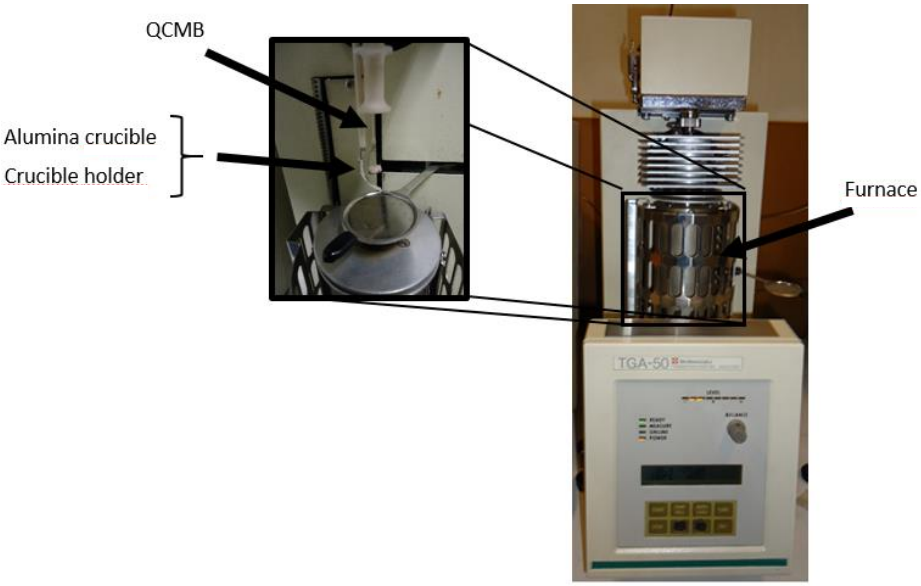

Figure 2.8 – Shimadzu TGA 50 TG Analyzer and its components. Highlighted: the furnace, the crucible with the sample for analysis and respective holder and the QCMB.

Sample weight variation ($\Delta m/\%$) is calculated according **Equation 2.6**:

$$\Delta m = \frac{w_{(t)}}{w_0} \times 100 \qquad \textbf{(2.6)}$$

where, $w_{(t)}$ and w_0 represent the desired weight in percentage at the time t, the registered weight in mg at the time t and the initial weight of the sample respectively.

Through the observation of the obtained thermogram, it is possible to infer how the thermal degradation of the sample unravels. There are five typical thermal degradation behaviours: decomposition with the formation of gaseous reaction products, occurring a single major to total weight loss due to decomposition and vaporization of the sample components; corrosion/metal oxidation, where a weight increase is verified due to the formation of non-volatile oxides; combustion, where an abrupt and fast weight increase is verified, due to the recoil caused by the sample's ignition, followed by its complete reduction (100-0%); multi-step decomposition, whose thermograms typically consist of the occurrence of more than one weight losses with the existence of a plateau in between them. This type of decomposition usually occurs when studying more complex samples (e.g. bacterial cellulose) that have different components, such as non-polymerized monomer, small oligomers and molecular structures, which can be degraded first followed by the polymer's backbone.

Another important set of data that is used, especially for the study of the kinetics of thermal decomposition, is the first derivative of the TGA curve which delivers more clear information about the decomposition steps given the fact their represented in the form of peaks which not only allows for the determination of the absolute temperature at the maximum weight loss rate (steepest slope of the weight loss curve) for each step but also check for possible overlapping decomposition reactions.

The expected TGA profile for BC is a multi-step decomposition, as already stated above, with the first step occurring within the range of 200-360 ºC and the second within 360-600 ºC. It is, however, important to note that these temperature ranges can vary since the thermal degradation behaviour is affected by the structural parameters of the material namely its orientation, crystallinity and molecular weight (Cheng *et al.*, 2009).

Relatively to the PPy expected TGA profile, its thermal decomposition is expected to be composed of one single step within the range of 200-600 ºC (Borthakur *et al.*, 2011).

Thermal decomposition kinetics

Parting from the data obtained from the TG analysis it is possible to determine the material's activation energy (E_{act}). The E_{act} was determined using the Kissinger's method (Sencadas *et al.*, 2011) which assumes that the reaction mechanism isn't well-known. This method uses the heating rate and the peak temperature values, which corresponds to the maximum thermal decomposition temperature (T_{max}) for the determination of the energy of activation.

Equation 2.7 describes the Kissinger's method (Kissinger, 1957):

$$\ln\left(\frac{\beta}{{T_p}^2}\right) = \frac{\ln(AE_{act})}{R} + \ln\left[n\left(1-\alpha_p\right)^{1-n}\right] - \frac{E_{act}}{RT_p} \qquad \textbf{(2.7)}$$

where β, α, Tp, A, R and n are the heating rate, conversion at maximum weight loss rate, absolute temperature at the maximum weight loss rate, the pre-exponential factor (min-1), the molar gas constant and the reaction order, respectively.

In order to determine the E_{act} from the TG data, the $\ln(\beta.(T_p^2)^{-1}$ is plotted *vs* $1000.T_p^{-1}$ as stated above and a linear regression is performed.

Experimental procedures

Thin bacterial cellulose films

Gluconacetobacter xylinus (ATCC 53582) was cultured in HS medium (Schramm and Hestrin, 1954) supplemented with 2% Corn Steep Liquor (a gift from COPAM – Companhia Portuguesa de Amidos, SA, Portugal) and a pH of 5.0. 100 mL of medium were inoculated and added to 200 mL Erlenmeyer flasks. The flasks were then incubated at a temperature of 25 ºC for 7 days. The resulting BC membranes were then washed thoroughly with distilled water and autoclaved at 121 ºC for 20 min. Finally, the washed membranes were cut into small strips of approximately 2 cm width and 5 cm length (**Figure 2.9A**) and some of them were freeze dried (**Figure 2.9B**) and stored in a desiccator for posterior usage on the CVD and WCP-β (*cf.* section below regarding the wet chemical polymerisation) processing methods. The average thickness and wet mass of the final films was 69.6 µm and 1 g respectively.

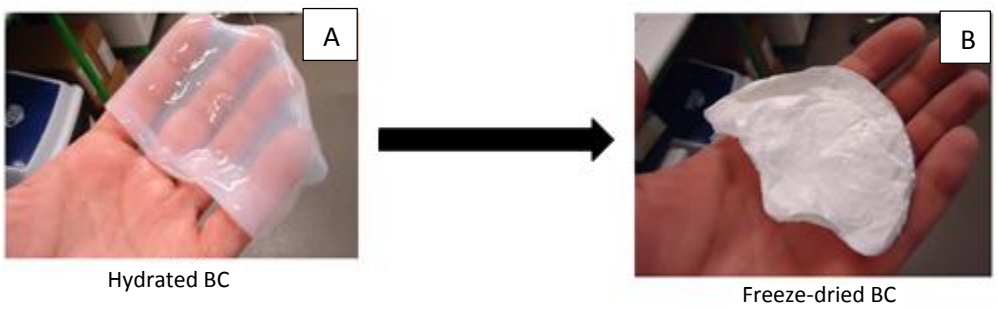

Figure 2.9 – Bacterial cellulose its different states – A: hydrated; B: freeze-dried.

Synthesis of BC-PPY membranes

Pyrrole monomer (Py, >98%) and ferric chloride (III) ($FeCl_3$) were purchased from Sigma and hydrochloric acid (HCl) was purchased from Panreac.

The bacterial cellulose-polypyrrole (BC-PPy) membranes were obtained through two different synthesis methods: chemical vapour deposition (CVD) of the pyrrole monomers on the BC membranes thus the polymerization of the pyrrole into PPy occurring in situ; and the wet chemical *in situ* polymerization. The selected oxidizing agent was ferric chloride and hydrochloric acid was used as a dopant. The used solvent

was water given that, according to the literature, the highest PPy conductivities are achieved using this solvent (Linford, 1990). **Figure 2.10** displays the aspect of the BC-PPy composites comparatively to pristine BC.

Chemical Vapour Deposition

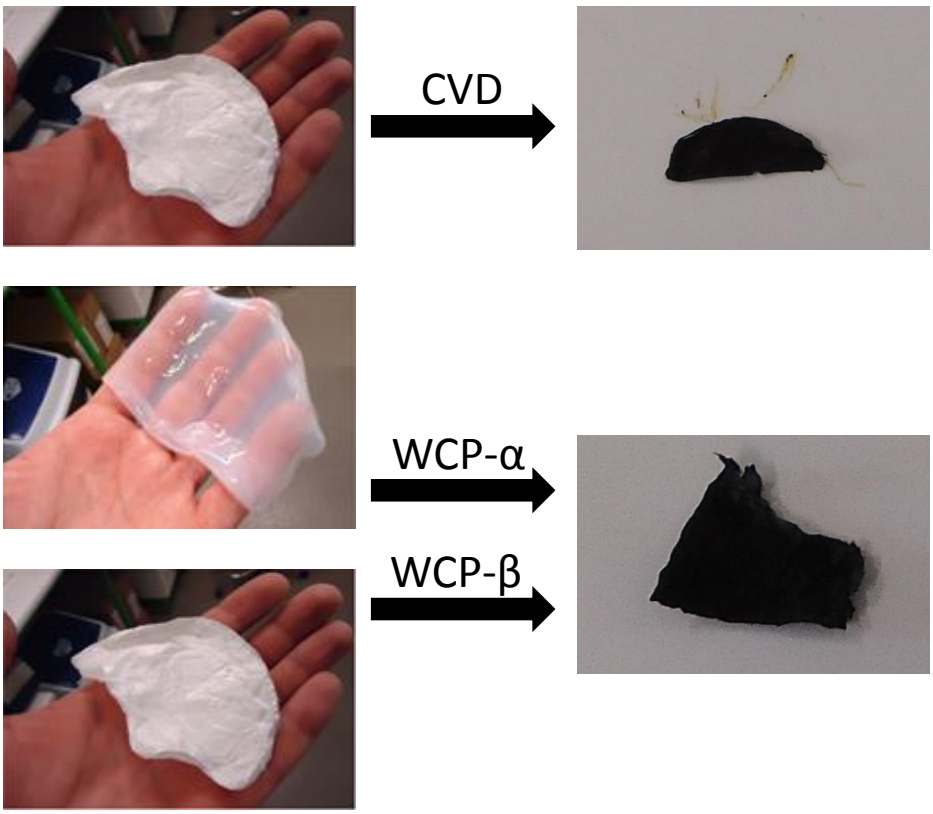

Figure 2.10 – Aspect of the BC-PPy composites comparatively to pristine BC.

For the CVD, three strips of freeze-dried BC of equal dimensions, as described above, per assay, (**Figure 2.9B**) were firstly impregnated with an aqueous solution of 7 mmol $FeCl_3$ and 1M HCl, at room temperature, under magnetic stirring at 100 rpm, to fulfil the oxidizing conditions necessary for the Py polymerization. The oxidized BC membranes were then placed in a desiccator and a >98% Py solution added in the bottom (**Figure 2.11**). The vessel was then closed and the air inside removed with a Millipore WP6122050 vacuum pump. Five polymerisation assays were performed with varying durations, specifically 40 minutes, 2, 6 and 8 hours. After each assay, the resulting BC-PPy composites were collected and washed in order to remove any excess PPy on the surface and dried at 60 º C overnight.

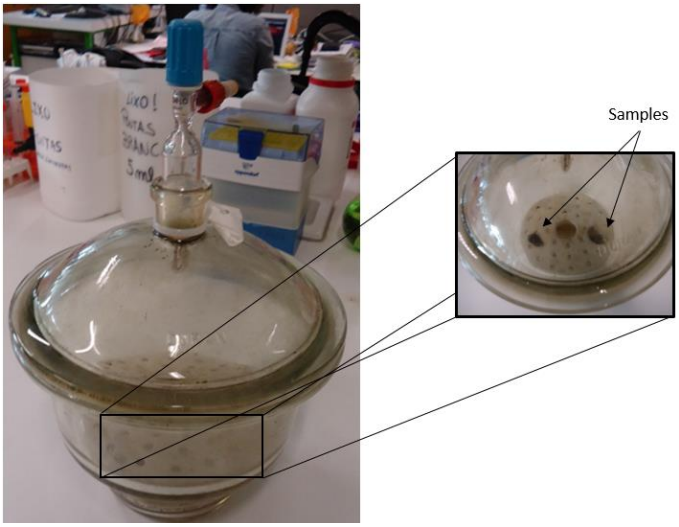

Figure 2.11 – Vessel used for the chemical vapour deposition (Panreac excicator). The samples were placed on the bottom of the vessel, as seen in the zoomed picture, and the vessel was posteriorly put in vacuum being the membranes exposed to the pyrrole vapours.

Wet chemical polymerization (WCP)

This method was based on the solution chemical polymerisation, however two variations were tested: a first one, WCP-**α**, consisting of the conventional method and a second one, WCP-**β**, where the freeze-dried BC strips were used instead.

WCP-α

For this method, three hydrated BC strips of equal dimensions, as described above, per assay, were placed in 100 mL of ultrapure water and 1 mL of Py was added per each 0.5 g of BC. After 30 minutes (to allow good impregnation of the BC with Py), a solution of 7 mmol of $FeCl_3$ and 16,8 mmol of HCl per 0.5 g of BC was added to fulfil the oxidizing environment conditions necessary for the Py polymerization. The aqueous system where the reaction occurred was placed in an ice bath, so that the polymerisation could occur at a temperature between 0 and 4 º C, with mechanical stirring of 100 rpm. Four assays were performed with the respective durations of 5 and 40 minutes and 2 and 6 hours. The resulting BC-PPy composites were thoroughly washed with ethanol and water in order to remove any PPy and unpolymerized Py excess and posteriorly freeze-dried.

Regarding the WCP-**β** method, the same steps were reproduced regarding the polymerisation.

Characterisation of the BC-PPY membranes

Electrical, mechanical and physicochemical properties were posteriorly characterized for the obtained BC-PPy composites, using electrical conductivity measurements, mechanical characterizations, scanning electron microscopy (SEM), thermogravimetric analysis (TGA), X-Ray diffraction (XRD) and Fourier Transform Infrared Spectroscopy by Attenuated Total Reflectance (FTIR-ATR).

Electrical conductivity measurements

All the synthesised BC-PPy membranes were analysed at least three times each, for the different polymerisation times and synthesis method, and the obtained resistivity and conductivity values were plotted versus the time of exposure in order to characterize the variation of the electrical properties according to the polymerisation time. The samples used had an approximate thickness of 7.6×10^{-5} m and the area of the analysed cross-section was of 1.96×10^{-3} m^2.

Two-point measurement technique

For the two-point measurement method, an electric voltage ranging from -1 to 1 V with increments of 0.1 V/s.

The R values obtained by linear regression of the IV curve were used to calculate the sample's electrical resistivity according to **Equation 2.1** and the conductivity was then determined by using $\sigma = \frac{1}{\rho}$.

Four-point collinear probe resistivity measures

An electrical current ranging from 0 to 10 µA with increments of 1 µA per measure was applied to the samples.

As for the two-point technique, a linear regression was applied to the IV curve and the slope of the trendline was used as the R value. The resistivity was then calculated using **Equation 2.3** and, finally, the conductivity was then determined using $\sigma = 1/\rho$.

Mechanical characterization

The samples that were characterized mechanically were BC, cBC-PPY and wBC-PPY. The mechanical tests were performed on a Linkam TST350 UTS (**Figure 2.5**) at 25 ºC and at the speed of 1 $mm.min^{-1}$.

Scanning Electron Microscopy (SEM)

A small fraction of the membranes were placed on a sample holder and then coated with a gold thin layer through sputtering (Polaran SC502) and were analysed on the SEM with an acceleration voltage of 15 kV under vacuum. The samples were analysed on surface and cross-section, in order to study the structure of the samples and if they were coated with PPy and if the PPy distribution was homogeneous throughout the composites bulk.

The diameter of the fibres was also measured using the ImageJ image edition program which allowed for the measurement of fibre diameter. 80 measurements were made in order to have a relevant number of values.

Fourier Transform Infrared Spectroscopy by Attenuated Total Reflectance (FTIR-ATR)

This technique was chosen to analyse the BC-PPy membranes because normal FTIR analyses gave no results as all the spectra were saturated (results not shown). Given this fact, the FTIR-ATR technique because such saturation does not happen as the IR beam only protrudes a small section of the sample when reflected through the ATR crystal instead of passing through the sample. The analysed samples were pure BC, freeze dried and dried, cBC-PPy and wBC-PPy, namely the initial and final polymerization times.

Table 2.1 represents the characteristic peaks for both PPy and BC (Wang *et al.*, 2013; Moosavi-Nasab and Yousefi, 2010).

Table 2.1 – Characteristic peaks of absorption for BC and PPy IR spectra.

BC		**PPy**	
wavelenght (cm^{-1})	Characteristic absorption band band	**wavelenght (cm^{-1})**	Characteristic absorption band
1058	C-O-C stretch	780	C-H wagging
1431	O-H bending	870	C-H wagging
1664	C=O stretching	1038	=C-H in plane bending
2999	C-H stretching	1165	C-N stretching
3415	O-H stretch	1292	=C-H in plane
		1454	C=C stretching
		1459	C-N stretching
		1539	C=C stretching
		3522	N-H stretching

X-Ray Diffraction (XRD)

The reason why this technique was chosen to characterize the BC-PPY membranes is because that, through comparison of the XRD pattern of the BC-PPY membranes and pure BC it is possible to assess if the modification of the BC fibres with the PPY affects the BC's crystalline structure.

Table 2.2 represents the characteristic diffraction peaks for both BC and PPy (Wang *et al.*, 2013).

Table 2.2 – Characteristic XRD diffraction peaks for BC and PPy.

BC	PPy
~14º	~27º
~17º	
~23	

Thermogravimetric Analysis (TGA)

In order to investigate if the PPy is chemically bound to the BC rather than just being deposited on its fibres, the thermal properties of the material, namely its thermal decomposition pattern and kinetics, i.e. activation energy, have been studied. For this purpose, a thermogravimetric analysis (TGA) was performed.

For the TGA performed during this experimental work, the TG analyser's model was a Shimadzu TGA-50 (**Figure 2.11**) and a 6.5 mm x 4 mm alumina crucible (highlighted in **Figure 2.11**) was used. The heat rates were 10, 20, 30 and 40 ºC/min, the maximum temperature was set to 800 ºC and the average weight of the analysed samples was ~1 ± 0.3 mg.

Statistical analysis

All assays were performed three times and the data as treated as mean ± standard error of the mean. Posteriorly, the data was treated statistically using the one-way analysis of variance with a Tukey post-test being the differences between the results considered statistically significant when p-values < 0.05.

Chapter 3. Results and Discussion

Morphological and electrical properties of the BC-PPy composites

Chemical Vapour Deposition (CVD)

This method was based on the work of Dall'Acqua (Dall'Acqua *et al.*, 2006), as applied in the preparation of electrically conductive textile fibres (namely viscose fabrics) through exposure of the fabrics to Py monomer vapours, followed by *in situ* polymerisation. The BC-PPy composites synthesised during this work were thus placed inside a closed vessel and vacuum sealed at room temperature, while in Dall'Acqua's method, the samples were placed on a closed vessel thermostated at 60 ºC. Despite these changes, both methods shared a common preparation step were the BC membranes were previously immersed in a $FeCl_3$ solution, to oxidise the BC membranes (oxi-BC). This step aimed at creating the oxidative environment necessary for the Py polymerisation.

Five assays were performed where different polymerisation times were experimented, namely 1, 2, 4, 8 and 12 hours respectively and the composites obtained through this method were labelled cBC-PPy. Posteriorly to the synthesis the composites they were analysed on the SEM microscope and had their conductivity assessed followed by a FTIR, XRD and TGA analyses. For the sake of clarity, FTIR, XRD and TGA will be discussed separately further bellow.

Scanning Electron Microscopy (SEM)

In order to verify the presence of PPy deposited in the BC matrix and the respective PPy coating of the fibres, the cBC-PPy composites were observed using the SEM technique.

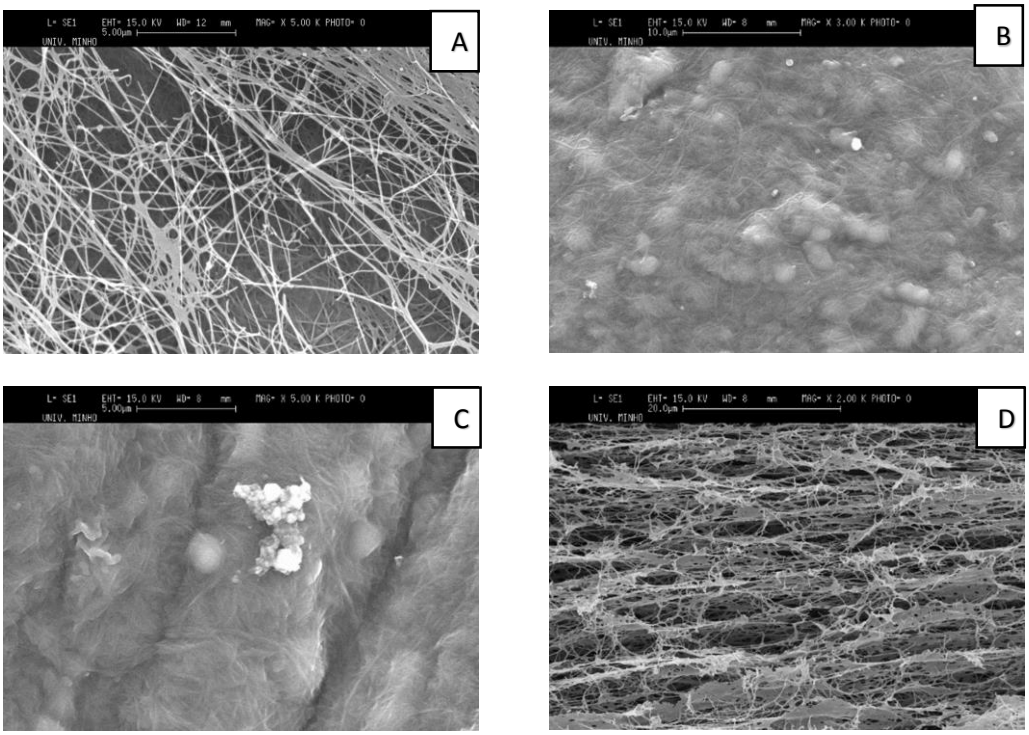

Figure 3.1 – SEM micrographs of pristine BC (A); cBC-PPy (1 hour) (B); cBC-PPy (8 hours) (C) and cBC-PPy cross-section (8 hours) (D).

Figure 3.1 displays a micrograph of pristine BC (**A**) and the cBC-PPy composites throughout the polymerisation reaction (**B** and **C**) namely at 1 hour and 8 hours. A micrograph of the sample's cross-section, after 8 hours of exposure to Py monomer is also shown (**D**). Based on the surface view (**A**, **B** and **C**), it is visible that the structure changes from a 3D-nanofibrilar network (**A**) to a bulky structure (**B** and **C**) where the fibres appear to be bound. The PPy cluster visible in micrograph **C** suggests extensive polymerization of Py on the exposed planes/faces by the CVD method. Interestingly, a cross-section observation of the polymerized sample (**D**), shows a more porous structure of the modified material. It is likely that this porous structure is associated with the freeze drying method as it is expected to preserve the 3D nanofibrilar structure of the BC matrix. Contrarily to the surface view figures, the cross-section area shows much lower polymer deposition hence confirming that the excessive polymerisation on the

membrane's surface hampers the further deposition of the monomer and posterior polymerization in the inner regions of the BC matrix.

As there are no BC-PPy composites obtained through this method in the literature, the main term of comparison are the composites obtained by Dall'Acqua *et al*. Despite the remarkable morphological differences between the bacterial cellulose and the viscose fabric fibres, having these a more organized cord-like structure and significantly larger sized-fibres, it is also possible to observe the presence of a PPy layer deposited on the viscose fibres under the form of clusters (**Figure 3.2**) (Dall'Acqua, 2006) as with the cBC-PPy. This is probably due to the viscose fibres having much more free space between them hence the condensation effect isn't verified and there is a wide distribution of the polymer.

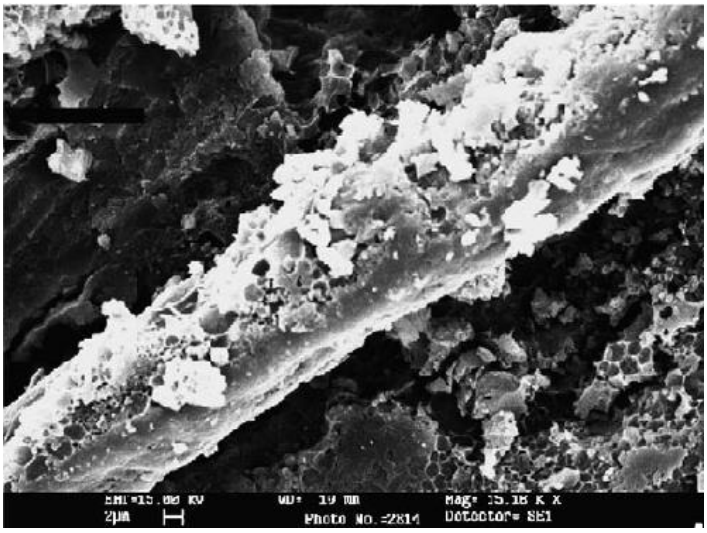

Figure 3.2 – SEM micrograph of the viscose-PPy composites obtained by Dall'Acqua *et al*. (2006).

Electrical properties

The Intensity-Voltage (IV) curves (**Figure 3.3A**) allowed to calculate the electrical conductivity of the BC-PPy composites. Conductivity measurements were taken with samples collected at different polymerization intervals.

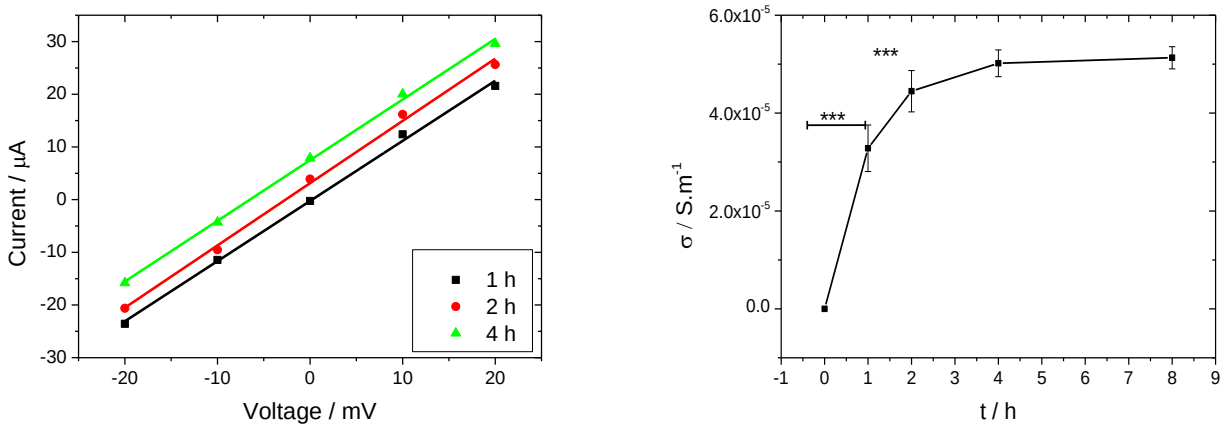

Figure 3.3 – A: IV curves obtained for the cBC-PPy composites; B: Condutivity of the cBC-PPy composites *versus* reaction time. Values are mean ± standard error of the mean of 3 independent experiments. * P ≤0,05, ** P ≤ 0,01 and *** P ≤ =0,001 in comparison with the previous point.

By looking at the obtained IV graphs it is possible to conclude that the material displays Ohmic conductivity given the fact that the graphs are linear and the voltage/current ratio is constant which means that the Ohm's law is obeyed and the resistance and, posteriorly, resistivity values can be obtained through a linear regression of the graph. The linear regression of the IV curves was then performed and the samples' resistivity (ρ) was calculated using **Equation 2.1.** The conductivity (σ) was then obtained by using $\sigma = \rho^{-1}$.

Figure 3.3B, by its turn, displays the different conductivities of the BC-PPy composites as a function of the exposure time to the PPy vapours.

The graph shown in **Figure 3.3B**, together with **Figure 3.1D**, confirms the presence of PPy in the cellulosic matrix. It is also clear that an accumulation of polymer occurs over time as result of a longer exposure to Py monomer which leads to a slight increase in the composite's conductivity between 1 and 4 hours of polymerisation being the highest increment registered between 0-2 hours, where the conductivity starts to hit its

cap at 4 hours. The fact that the conductivity of the composites stabilizes at 4 hours is due to the saturation of PPy on the membrane's surface which blocks the further deposition of the polymer on the inner layers of the BC.

It is noteworthy, though, that despite the conductivity displayed by the composites obtained through the CVD method being fairly low, these composites can be considered as semi-conductors as their σ is in the range of 10^{-10} to 10^{1} $S.m^{-1}$ (*cf.* **Figure 1.5**) being located in the beginning of this class of semi-conductive materials.

It is impossible to make a direct comparison between cBC-PPy composites and the viscose-PPy in terms of conductivity as the authors did not publish any specific values. It is, however, possible to infer that the BC-PPy composites may have comparable conductivities by looking at the IV curves and inferring the conductivities by extrapolating the data presented on the publication made by Dall'Acqua *et al*. (2006).

Wet Chemical Polymerisation (WCP)

In the method described by Wang *et al.* (2013), originally, the polymerisation occurs in solution by immersing BC membranes on a mixture of water and dimethyl formamide (DMF) and adding Py monomer and $FeCl_3$ and HCl to the solution (Wang *et al*., 2013). The resulting BC-PPy composites were then washed thoroughly with water and ethanol and freeze-dried. This method showed potential towards the synthesis of highly conductive BC-PPy composites with conductivities as high as 70 $S.m^{-1}$. This method was then adopted as a comparative methodology to the chemical vapour deposition method.

The WCP method was tested in two scenarios: firstly, hydrated BC membranes were used and, secondly, freeze-dried BC membranes were used. This variation aimed at verifying if the removal of water from the membrane, increasing its porosity, would allow better diffusion of Py into the interior of the BC matrix.

The polymerisation times were 5 and 40 minutes, 2 and 6 hours respectively. Finally, these composites, labelled wBC-PPy-α (traditional method) and wBC-PPy-β (when freeze-dried BC is used) were analysed using the same techniques that were used

for the analysis of the cBC-PPy ones (SEM, FTIR, XRD and TGA). For the sake of clarity, FTIR, XRD and TGA will be discussed separately further bellow.

WCP-α

Scanning Electron Microscopy (SEM)

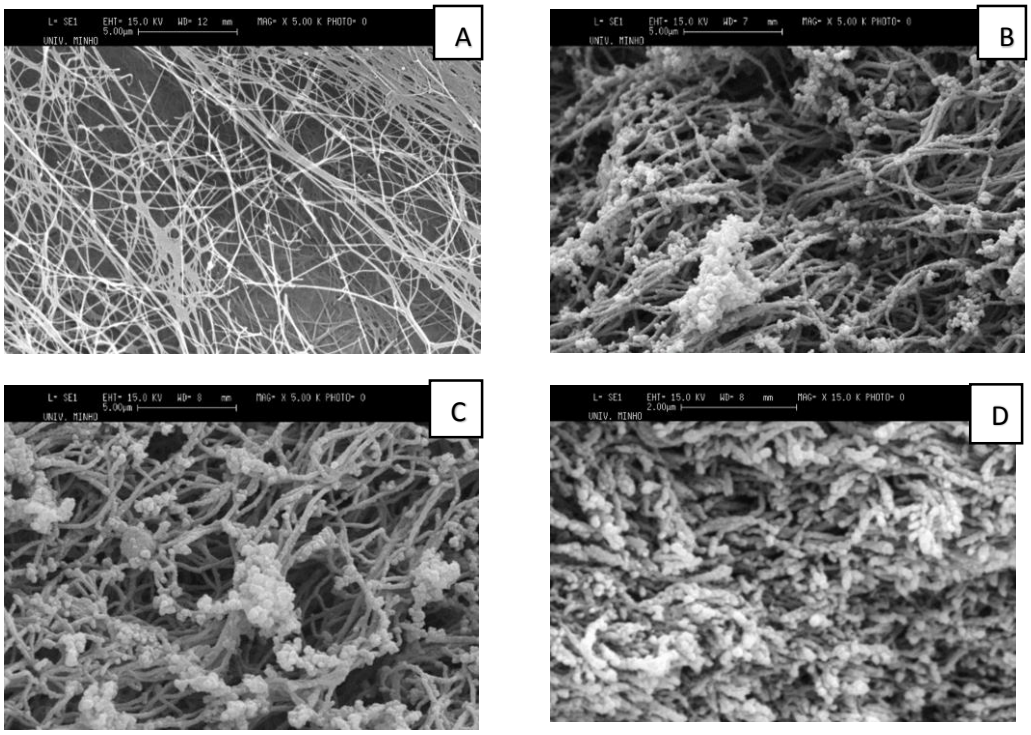

Figure 3.4 – SEM micrographs of pristine BC (A); wBC-PPy-α (5 minutes) (B); wBC-PPy-α (6 hours) (C) and wBC-PPy cross-section (D).

Figure 3.4 displays the SEM micrographs of the BC-PPy composites obtained through the WCP-α method (**B** and **C**) at different times, 5 minutes and 6 hours respectively. A micrograph of pristine BC (**A**) is also shown for comparison. By observing the SEM micrographs, it is visible that the wBC-PPy-α composites display a porous structure, much more than the cBC-PPy composites (**Figures 3.4B and C**) obtained by CVD. Also, the cellulose fibres are coated by a relatively dense PPy layer thus being visible an increment in the fibre's diameter due to the deposition of this PPy layer. This increment in the fibre diameter is slightly higher the more time the polymerisation lasts being as more PPy is added to the fibre coating being the most relevant increase verified right in the beginning of the reaction, at 5 minutes, being a rise of *circa* 300 nm

registered. **Figure 3.5** displays the measured fibre diameters of the different analysed for comparison.

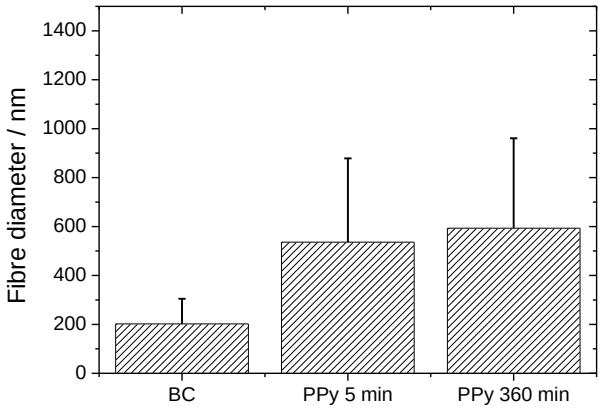

Figure 3.5 – Fibre diameter increase throughout the reaction

Through the observation of **Figure 3.5,** a high variability among the fibre diameters can be seen given the standard deviations, this is due to the fact, despite that 80 measurements were made, there is a relevant level of heterogeneity between the fibres as it can be seen on the SEM.

The distribution of the PPy throughout the BC matrix is also qualitatively confirmed by observing cross-section micrographs of derivatized BC. As it can be observed in **Figure 3.4D,** BC fibres appear to be fully coated with a PPy layer. Comparatively to the composites obtained by Wang, wBC-PPy-α composites display a similar PPy coating that is, however, slightly denser and more heterogeneous (**Figure 3.6**).

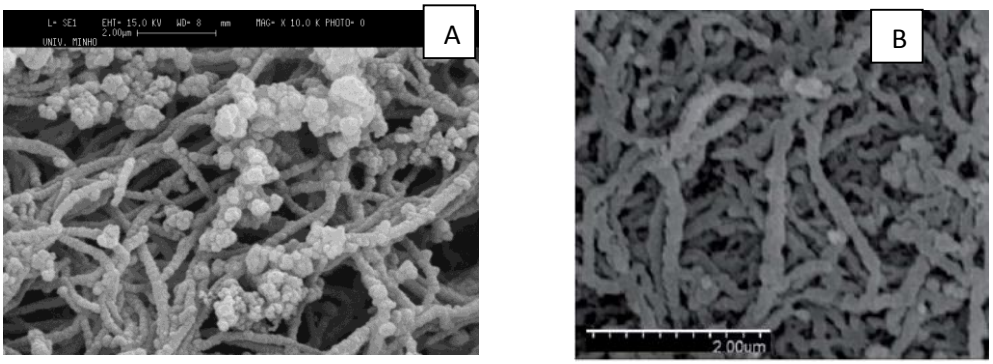

Figure 3.6 – SEM micrograph of wBC-PPy-α (6 hours) (A) and FESEM micrograph of BC-PPy composites obtained by Wang *et al*. (2013) (6 hours) (B).

Electrical properties

Figure 3.7A displays examples of the IV graph for the different reaction times for the first variation of the WCP method (WCPα) whereas **Figure 3.7B** displays the different conductivities of the wBC-PPy-α throughout the modification process.

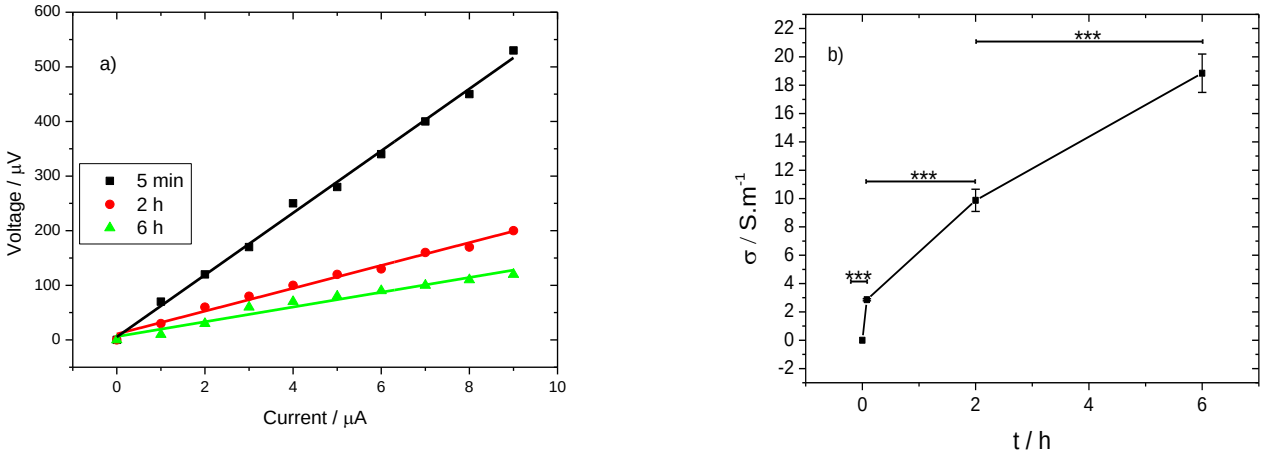

Figure 3.7 – A: IV curves obtained for the wBC-PPy-α composites; B: Conductivity of the wBC-PPy α composites *vs* reaction time. Values are mean ± standard error of the mean of 3 independent experiments. * P ≤0,05, ** P ≤ 0,01 and *** P ≤ =0,001 in comparison with the previous point.

Through the observation of the IV graph, it is possible to conclude that, as with the CVD method, the wBC-PPY-α composites display Ohmic conductivity and the resistance values are obtained through the linear regression of the graph.

The samples' resistivity (ρ) and conductivity (σ) were then calculated by using **Equation 3.2** and $\sigma = \rho^{-1}$ respectively.

Figure 3.7B shows the increase of the composites' conductivity with the polymerisation time. The electrical conductivity of these composites is higher than the cBC-PPy ones, as will be further shown in the next sub-chapter. These composites are also in placed in the semi-conductors class being, however, located in the borderline between the semi-conductor and conductor class, given the high conductivity values recorded.

Comparatively to the composites obtained by Wang *et al* (2013), the wBC-PPy-α composites display is nearly 50 $S.m^{-1}$ lower conductivity despite having a denser PPy

coat, as already visualized by SEM microscopy. However, compared to other BC-PPy composites obtained with a similar method in the literature, namely the ones obtained by Muller *et al*., the wBC-PPy-α composites have a nearly seven fold higher conductivity (2.7 $S.m^{-1}$ *vs* 14 (*cf.* **Table 3.1** below, where a comparison between the obtained composites and the ones in the literature is made).

WCP-β

Scanning Electron Microscopy (SEM)

On **Figure 3.8**, it is possible to observe the SEM micrographs of pristine BC (**A**) and the BC composites obtained through the WCP-β method (**B** and **C**) for 5 minutes and 6 hours of polymerization respectively.

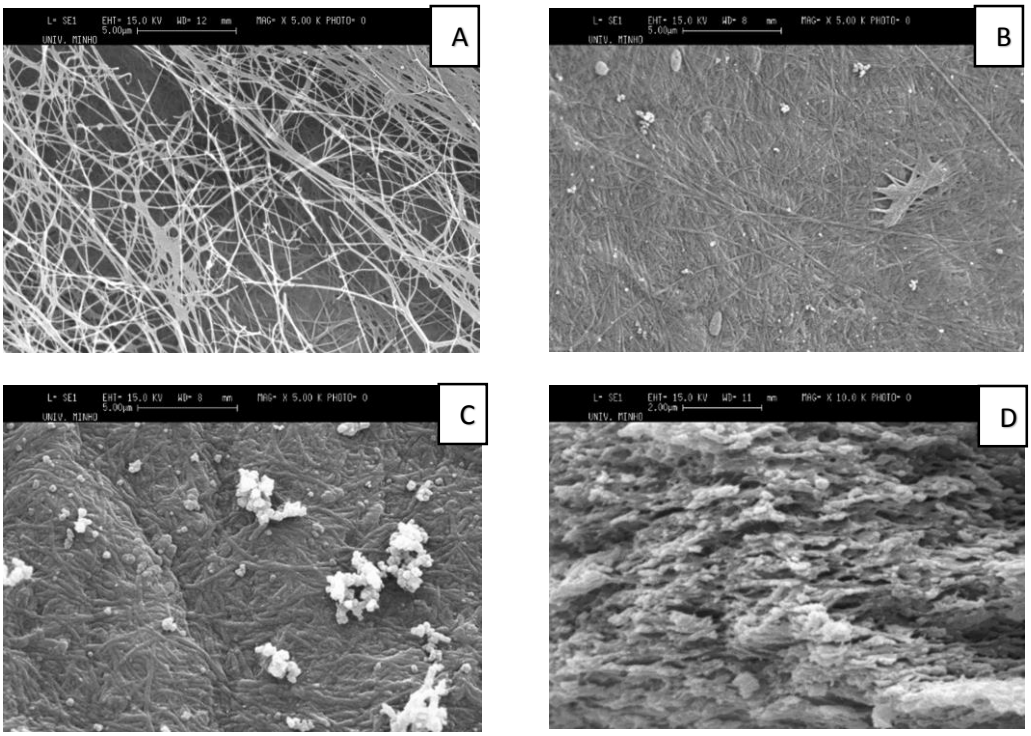

Figure 3.8 – SEM micrographs of pristine BC (A); wBC-PPy-β (5 minutes) (B); wBC-PPy-β (6 hours) (C) and wBC-PPy-β cross-section (8 hours) (D).

Through the observation of the micrographs, the most remarkable aspect is the bulky aspect of the samples: it is possible to see that the BC nanofibres are completely and highly coated with PPy. From top planar view, qualitative observation of the micrographs show that the thickness of the fibres increases with the polymerization time. This can possibly be the reason for the bulky aspect of the membranes.

On a hydrated BC membrane, Py must first go through a diffusional process into the bulk of the BC matrix so that polymerization can then occur. Using a freeze-dried BC membrane, by its turn, an easier Py better diffuses into the bulk of the matrix occurs as the membrane hydrates in the Py aqueous solution, subsequently allowing for a more extensive polymerising inside the BC matrix thus forming thicker layers. This becomes clearer through the observation of the micrograph of the samples at 10.000X (**Figure 3.9**) where the fibres become closer to each other as more and more PPy is formed around the nanofibres.

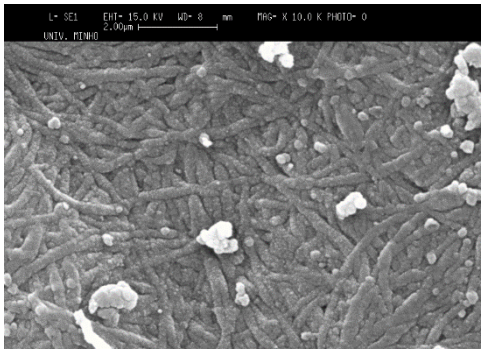

Figure 3.9 – SEM micrograph of wBC-PPy-β (6 hours) with a 10.000x.

The formation of PPy clusters on the surface of the composite is also observable, becoming these clusters bulkier with the polymerization time (data not shown). Despite the wBC-PPY-β composites displaying a much less porous structure as the wBC-PPy-α ones, it is acknowledgeable, by observing micrograph **D**, that PPy is distributed throughout the whole BC matrix as PPy-coated fibres are visible. This further suggests that by freeze drying polymerization around the BC nanofibers was further promoted, in contrast to a polymerization with hydrated BC (never-dried BC).

Electrical properties

Figures 3.10A displays examples of the IV graphs for the different reaction times for WCPβ composites. **Figure 3.10B**, by its turn, displays the IV graphs only for 2 and 6 hours as they were overlapped in **Figure 3.10A** due the difference in the voltage values.

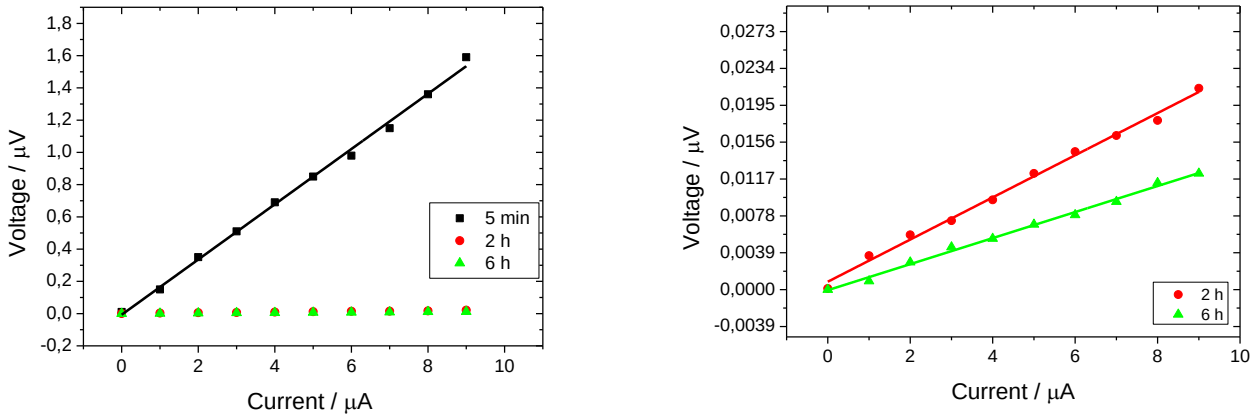

Figure 3.10 – A: IV curves obtained for the wBC-PPy-β composites; B: IV curves obtained for the wBC-PPy-β composites (5 minutes excluded).

Similarly to cBC-PPy and wBC-PPY-α, the wBC-PPY-β composites display Ohmic conductivity and the resistance values were obtained through the linear regression of the graph. As with wBC-PPY-α, the samples' resistivity (ρ) were calculated by using **Equation 4.2** and the conductivity (σ) by using $\sigma = \rho^{-1}$.

Figure 3.11, by its turn, displays the different conductivities of the wBC-PPy-α composites throughout the modification process.

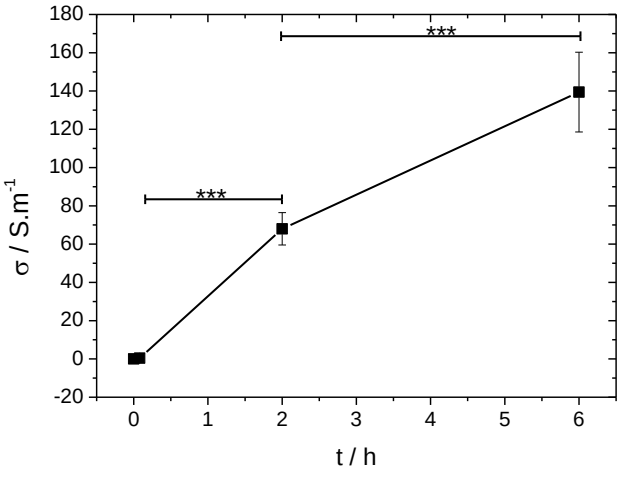

Figure 3.11 – Conductivity of the wBC-PPy-β composites *versus* reaction time. Values are mean ± standard error of the mean of 3 independent experiments. * P ≤0,05, ** P ≤ 0,01 and *** P ≤ =0,001 in comparison with the previous point.

As with all the previously analysed composites, the electrical conductivity of wBC-PPy-β composites increases with the polymerization time. Regarding to electrical conductivity, these composites, specifically the wBC-PPy-β 6h, fit in the conductor class (*cf.* **Figure 1.5**). When compared to cBC-PPy and wBC-PPy-α, the wBC-PPy-β composites display higher conductivities compared to cBC-PPy and *circa* 7 fold higher than wBC-PPy-α as it will be detailed below. Finally, comparatively to the composites obtained by Wang *et al*. and Muller *et al*., these composites display higher conductivities as well, namely 2 and *circa* 54 fold respectively.

The higher conductivities displayed by these composites are related to, first of all, the addition of the freeze-drying step at the beginning of the process which, as explained above on the SEM analysis, allowed for an easier intrusion of the polymerisation medium into the BC matrix thus leading to an easier coating of the fibres and, consequently, the formation of a thicker PPy coating.

Comparison between the three methods

Morphology

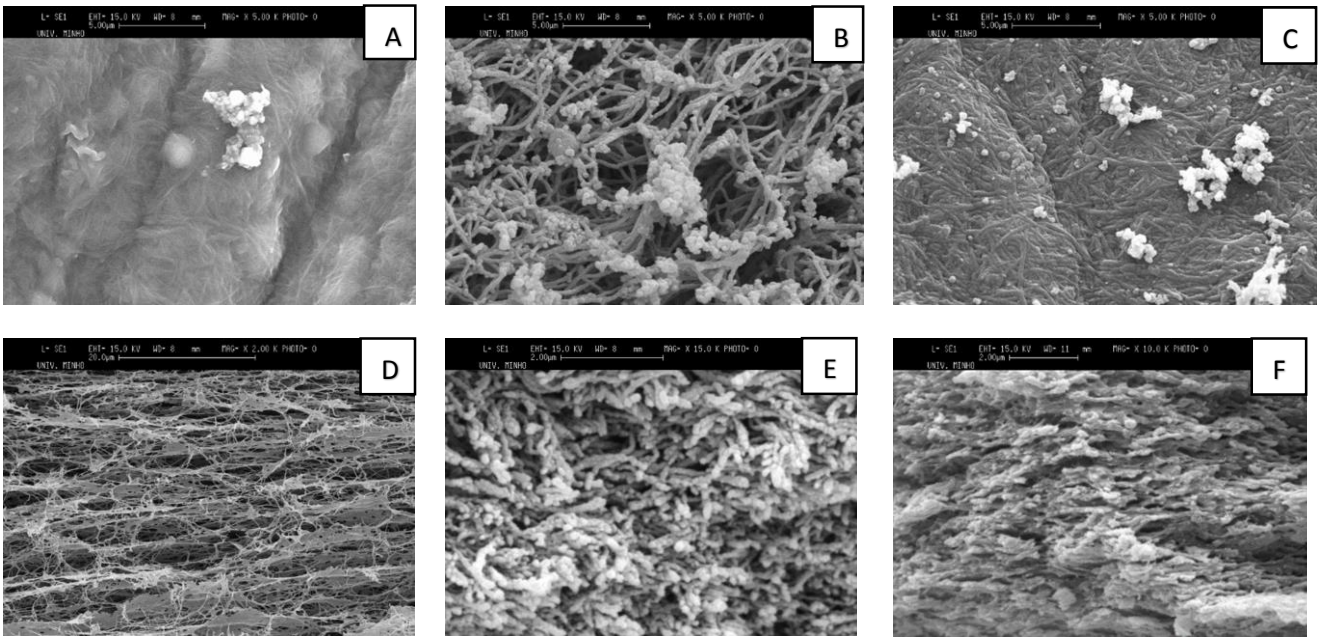

Figure 3.12 – SEM micrographs of cBC-PPy (8 hours) (A); wBC-PPy-α (6 hours) (B) and wBC-PPy-β (6 hours) (C) and their respective cross-sections (D, E,F)

Figure 3.12 above displays the SEM micrographs for the three different BC-PPy composites obtained throughout this research: cBC-PPy (**A**); wBC-PPy-α (**B**); wBC-PPy-β

(**C**) at the final polymerisation times (8 hours for cBC-PPy and 6 hours for both wBC-PPy-α and β). A clear difference is visible between the cBC-PPy and wBC-PPy composites' morphologies which resides in the different drying methods that were used. Between both the composites obtained through the WCP processing method there are also distinct differences between their morphologies; the wBC-PPy-β composites have a bulky aspect, however, it is possible to distinguish the presence of the fibres which look thicker. It is important to remember that, for the wBC-PPy-β composites the BC membranes were freeze-dried before and after the polymerisation while in the wBC-PPy-α ones the used BC was maintained hydrated, which can influence the resulting composite's morphology. This can explain the swelled aspect of the second composites as more polymer was assembled on the fibres thus increasing their diameter more than in the first composites which leads to less space between the fibres hence the bulky aspect. Regarding the PPy clusters that assembled on the wBC-PPy-β composites' surface, this is due to saturation of the polymer on the fibres thus leading to accumulation on its surface.

Electrical conductivity

In order to compare the conductivity displayed by the composites obtained by the three tested methods a bar chart (**Figure 3.13**) in which the conductivities for the CVD, WCPα and WCPβ at 2 hours of reaction time (the only time that is common to all methods) were plotted side-by-side.

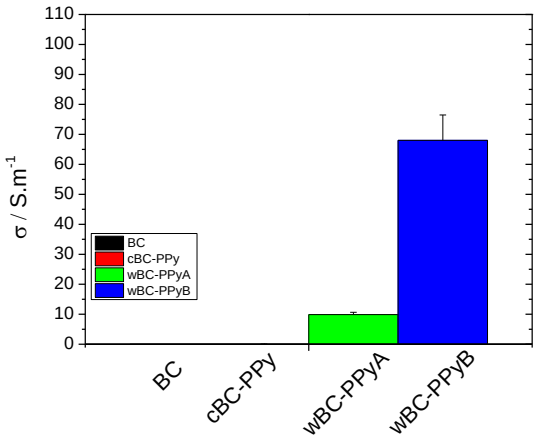

Figure 3.13 – Comparison between the conductivity of the two different BC-PPy composites.

Through the observation of the graph it is possible to ascertain a remarkable difference between the cBC-PPy composite's conductivity and the wBC-PPy ones ($5x10^{-5}$ $S.m^{-1}$ *vs* 19 and 140 $S.m^{-1}$).

Relatively to the WCP method, comparing both variations, it is possible to conclude that additional freeze-drying step prior to the polymerisation reaction improves the conductivity of the resulting composites. This is due to the removal of the water molecules in the spaces between the fibres allowing a better intrusion of the Py due to higher absorption of the reaction medium by the cellulose as opposed to what happens in the first variation were the BC membranes are soaked-wet thus being leading to a more difficult assembly of the Py monomer on the BC matrix. However, this doesn't happen with the cBC-PPy composites even these bearing a similar morphology and non-porous structure. This probably happens due to a slow intrusion of the Py monomers on the cellulose matrix due to lower quantity as this method is limited to the amount present in the vapour and due to possible condensations of the Py vapour on the membranes' surface which causes higher saturation on the membrane's surface hence difficulting the diffusion of higher amounts of Py into the matrix as it can be seen in **Figure 3.1.**

Additionally, a small test was performed, where a very simple circuit composed of a 9V battery, a LED and a BC-PPy strip was constructed in order to turn on the LED light by making an electrical current pass through the BC-PPy composite. This test, as expected, was successful and the LED was turned on as electrical current passed through the BC conductive composites. Interestingly, the difference in conductivity between the cBC-PPy and wBC-PPy composites could be visually observed as well, since the emitted

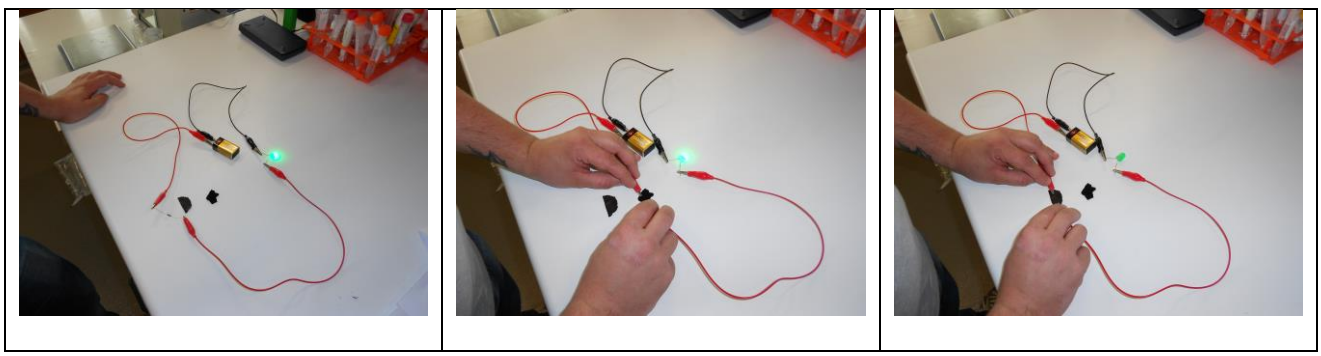

Figure 3.14 – Demonstration of an electrical circuit where a LED light was turned while integrating the wBC-PPy (B) and cBC-PPy (C) composites in the circuit. A resistance of 100 Ω was also used as reference (A).

light was much stronger when the wBC-PPy composite (which had higher conductivity) was used (**Figure 3.14A**), comparatively to cBC-PPy one (**Figure 3.14B**). A circuit with a 100 Ω resistance (**Figure 3.14C**) was also performed as a term of comparison – the light's luminosity was very comparable to this 100 Ω resistance circuit, when the wBC-PPy composite was used (figures A and C).

Finally, when compared to other composites obtained by other publications (as summarized in **Table 3.1**, below), the composites that were synthesised during this work have comparable and, in the case of the wBC-PPy-β composites, even higher conductivities. The cBC-PPy composites, despite being synthesised by a different method, can be compared with the composites obtained by Dall'Acqua and with other works that used different textiles for the synthesis of this sort of composites such as the ones obtained by Macasaquit and Binag (Macasaquit and Binag, 2010) where polyester (PET) fibres were used. The conductivities of cBC-PPy composites are, overall, comparable to some of the PET-PPy composites' conductivity which is in a range between 2.45×10^{-5} and 6.89×10^{-2} $S.m^{-1}$.

As for the composites obtained through the WCP methods, as already referred above, their conductivities are comparable with the ones obtained by Wang *et al.*, except for the β compounds which have a two-fold higher conductivity, and much higher than the ones obtained by Muller *et al*. being the wBC-PPy-β composites the ones with the highest electrical conductivity comparatively to all the current available information on BC-ICP composites. It is also noteworthy to mention that the conductivity exhibited by these composites is within the range of the ones exhibited by Silicon and Germanium (*cf.* **Figure 2.5**) which are commonly found in the vast majority of electronics. **Table 3.1** displays a list with different composites found in literature and their respective conductivities as well as the cBC-PPy and wBC-PPy-α and wBC-PPy-β composites for comparative terms.

Table 3.1 – σ of different BC-PPy and textile-PPy composites in the literature.

Composite	σ (S.m^{-1})	Refference
PET-PPy	2.45x10^{-5} to 6.89x10^{-2}	(Macasaquit and Binag, 2010)
BC-PPy	20 to 80	(Wang *et al*., 2013)
BC-PPy	7.8x10^{-7} to 2.7	(Muller *et al*., 2013)
cBC-PPy	3.5x10^{-5} to 5x10^{-5}	
wBC-PPy-σ	3 to 19	
wBC-PPy-β	60 to 140	

In short, the obtained compounds have conductivities that are comparable and, in most of the cases, higher than other composites which are composed of textile or BC fibres and PPy. It is also relevant to notice that, when using three different processing methods, three different types of composites can be obtained, all with varying conductivities and morphologies which translates into high versatility towards the development of applications. The graph displayed by **Figure 3.15** displays the evolution of the electrical conductivity of the different BC-PPy composites taking into account the different processing methods and polymerisation time.

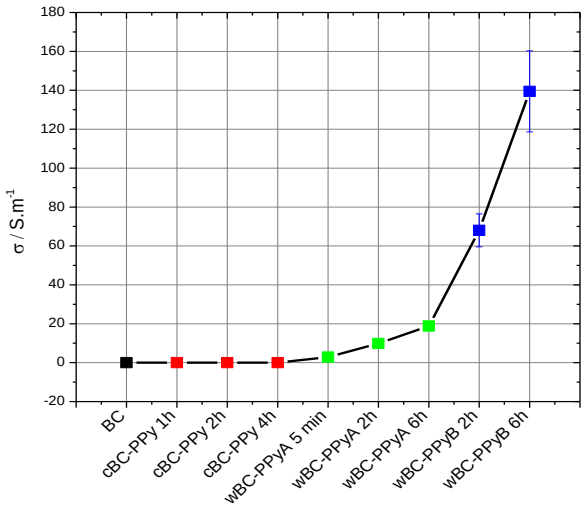

Figure 3.15 – Evolution of the BC-PPy composites' conductivity according to the used processing method and polymerisation time.

Structural and mechanical characterization of the composites

In order to further characterize the BC-PPy composites' surface and structural properties, FTIR-ATR and XRD analyses were performed. The samples were also submitted to tensile testing in order to study the effect of the processing on the samples' mechanical properties.

Fourier Transform Infrared Spectroscopy by Attenuated Reflectance (FTIR-ATR)

The FTIR spectra of both the BC, PPy and the BC-PPy composites are shown in **Figure 3.16**. **Figure 3.16B**, which corresponds to the PPy IR spectrum is displayed separately as the transmittance values (T/arbitrary units (a.u.)) were much lower than the ones of BC and BC-PPy and the spectrum were more difficult to attain. No distinction is made between the composites obtained through the different methods as they all displayed similar IR spectra (data not shown), being the presented spectrum correspondent to the wBC-PPy spectrum as it had the best visibility.

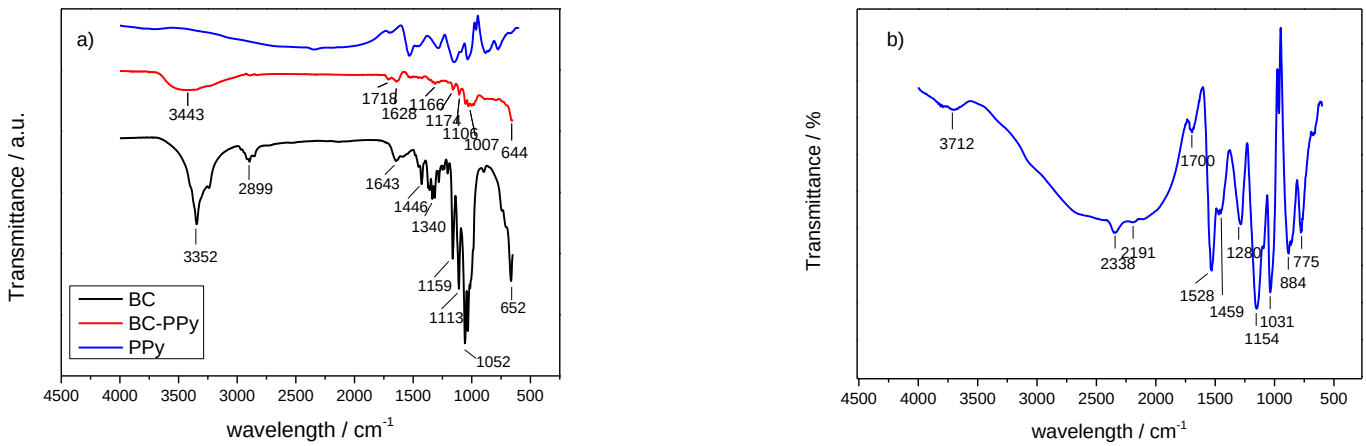

Figure 3.16 – A: BC, PPy and BC-PPy IR spectra; B: Amplified PPy IR spectrum.

By analysing the BC spectrum, the characteristic IR peaks (*cf.* **Table 2.1**) for the bacterial cellulose are visible, namely a broad band attributed to the O-H stretch

vibration at 3352 cm^{-1} and a band at 2899 cm^{-1} corresponding to the C-H stretch. A peak corresponding to carbonyl functional group, namely a C=O stretching, can also be seen at 1643 cm^{-1} as well as a steep band attributed to C-O-C stretching at 1052 cm^{-1}. The PPy spectrum, by its turn, also agrees well with the literature and the characteristic peaks (*cf.* **Table 2.1**) being a broad band seen at 3712 cm^{-1} which corresponds to the N-H stretch, a band at 1528 cm^{-1} attributed to the C=C stretch, the C-N stretching, in the pyrrole ring, is also visible at 1459 cm^{-1} as well as the C-H and C-N in-plane ring bending, at 1280 cm^{-1} and 1164 cm^{-1} respectively. Regarding the BC-PPy composites' spectrum, a N-H stretching band, very similar to the one seen in the PPy spectrum, can be seen at 3443 cm^{-1} rather than an O-H stretching band at 3352 cm^{-1} which is quenched, as well as the C-H stretching band at 2899 cm^{-1}. The presence of this N-H stretching and the quenching of both the O-H and C-H stretches reinforce the conclusion that the BC fibres are coated with the PPy. On the BC-PPy spectrum it is also possible to observe two bands attributed to the C=C of the Py ring stretching, at 1718 and 1628 cm^{-1}, and a weak band at that corresponds to the C-N stretching at 1007 cm^{-1} while occurring the quenching of the steep 1052 cm^{-1} C-O-C stretch observed in the BC spectrum. This is also verified on other BC-PPy composites obtained by other authors were the BC-PPy composites' spectra share peaks from both BC and PPy IR spectra (Muller *et al.,* 2013 and Wang *et al.*, 2013).

X-Ray Diffraction crystallography (XRD)

Regarding the XRD analysis, it is shown in **Figure 3.17** the patterns for pure BC, PPy and BC-PPy. As with the FTIR-ATR, no distinction was made between the BC-PPy as all obtained spectra were identical (data not shown), belonging the present XRD pattern to the wBC-PPy composites. By analysing the BC patterns, the three main characteristic peaks (*cf.***Table 2.2**) for pure BC, namely at 14.18º; 16.74º and 22.6º which correspond to the ($1\ \overline{1}\ 0$), (1 1 0) and (2 0 0) cellulose's diffraction planes respectively, are visible. The characteristic (*cf.* **Table 2.2**) broad peak of PPy, which translates as the material being amorphous, is also visible at 26.61º as expected (Wang *et al.*, 2013).

Regarding the BC-PPy composites it is visible that the BC peaks disappear almost completely, becoming much more tenuous on the XRD pattern, as marked by the circled

areas. Overall, the pattern corresponds to an amorphous material, having some similarity to the PPy pattern (to the exception of the broad peak at 26.61º being unnoticeable). This reinforces the conclusion that cellulose fibres are completely coated by PPy (Wang *et al.*, 2013).

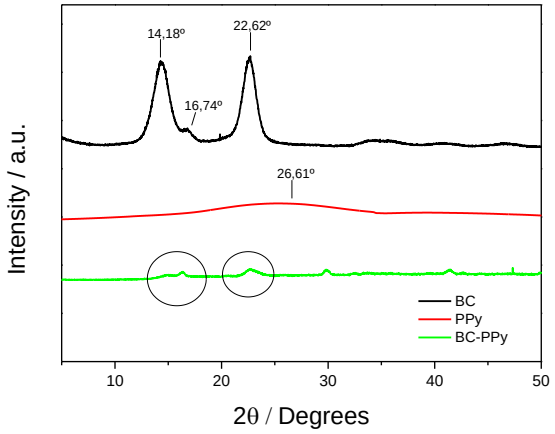

Figure 3.17 – BC, PPy and BC-PPy XRD diffraction patterns.

Mechanical properties

Regarding the mechanical characterization of the samples, **Figures 3.18** displays the stress-strain curves for BC, cBC-PPy 5 min and cBC-PPy 2 h. The stress-strain curves for the wBC-PPy composites can't be represented as it was impossible to perform tensile tests on these samples: these were extremely brittle and would break right at the beginning of the test.

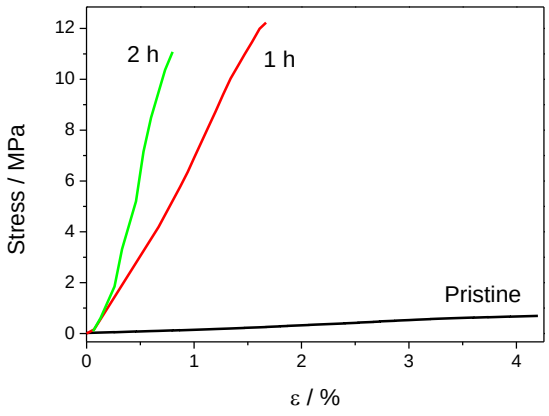

Figure 3.18 – Stress-strain curves of the BC and cBC-PPy composites.

By looking at the presented stress-strain curves it is visible that the BC-PPy composites display fairly weaker mechanical properties and have much less elasticity as they break when half of the strain (2% for the BC-PPy *vs* 4% for the BC) is applied and high stress values are registered.

Table 3.2 shows the strain (ε/%) and stress (MPa) values at the break point as well as the elasticity moduli for each of the samples.

Table 3.2 – Comparison between the BC and BC-PPy's mechanical properties.

	Strain @ Break (%)	Stress @ Break (MPa)	Young's Modulus (GPa)
BC	7.983 ± 1.585	0.983 ± 0.468	24.284 ± 7.947
cBC-PPy 1 h	1.113 ± 0.543	6.340 ± 0.057	872,.260 ± 63.576
cBC-PPy 2 h	0.735 ± 0.092	10.130 ± 1.344	1497.450 ± 136.825

By observing and comparing the different values presented on **Table 3.2** it is visible that the polymerization time strongly deteriorates the mechanical properties of the composites. Despite the visible increment in the Young's modulus, which indicates that the material becomes stiffer throughout the process hence being necessary a higher load to deform it, the material is not mechanically strong as it is permanently deformed with a small load.

This deterioration is probably due to degradation of the fibres given the oxidation and the abrasive environment in which the polymerisation occurs, which is very acidic due to the presence of the $FeCl_3$ and HCl, in the case of the WCP method whose obtained composites, by their turn, are even more brittle and couldn't even be tested as it was stated above. The deposition of PPy and possible resulting interactions between the polymer and the fibres may also be causing this deterioration which corroborates with the XRD results where it can be seen that the material becomes amorphous hence tending to be weaker.

It is, however, important to note that these mechanical characteristics are far better than the PPy's itself, which, being a powder, has no mechanical resilience at all.

Thermogravimetric Analysis (TGA)

In order to study the thermal degradation of the samples as well as evaluate the possible interactions between the bacterial cellulose and the PPy on the BC-PPy composites a thermogravimetric analysis was performed for the BC, PPy and BC-PPy composites followed by a study of the decomposition's kinetics.

The thermograms for the decomposition of BC, at all the heating rates of 10, 20, 30 and 40 ºC.min^{-1} and their respective derivatives are shown by **Figures 3.19, 3.20** and **3.21** respectively. **Figures 3.19B, 3.20B** and **3.21B,** by their turn, display the derivatives of the TG curves which provide useful information towards the study of the thermal degradation kinetics as their peaks correspond to the maximum temperature value registered for each thermal degradation step, which is used on the Kissinger's equation (**Equation 2.7**).

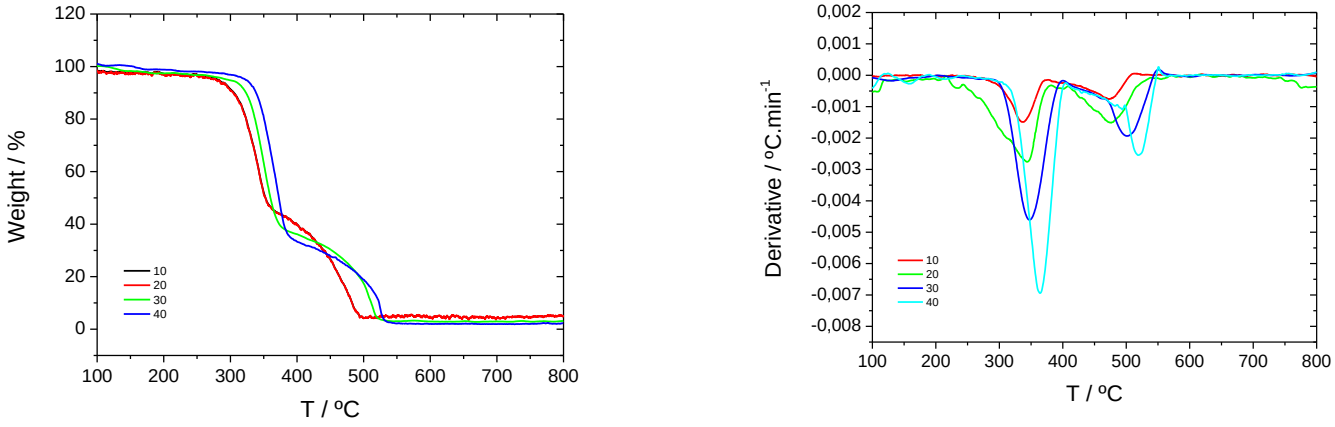

Figure 3.19 – A: BC TGA curve; B: Derivative of the BC TGA curve.

By observing the BC thermogram (**Figure 3.19**), firstly, a small mass loss is visible up to 150 ºC, due to the removal of residual adsorbed water can be seen even after the water being removed from the material.

Secondly, BC's thermal decomposition follows a multi-step model where two distinct steps are distinguishable in the ranges between 200-400 ºC and 450-600 ºC. These decomposition steps agree well with the typical decomposition steps described for the thermal decomposition of BC found in the literature (Cheng *et al.*, 2009)

corresponding the first step to the removal of small oligomeric fragments and the second step to the breakage of the polymeric chains which, by their turn, are strongly linked by very stable ligations which require high energies in order to break.

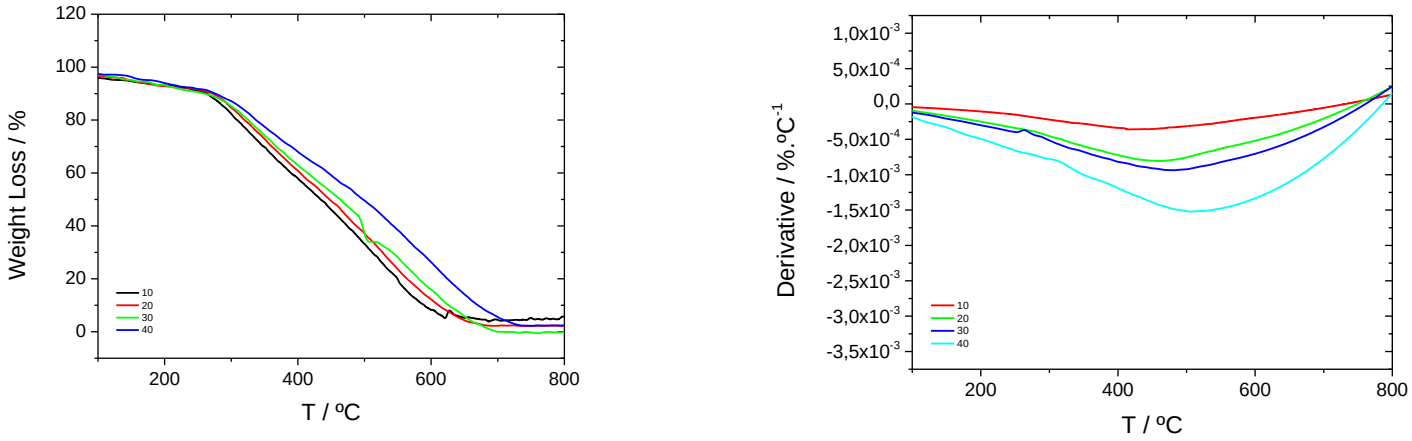

Figure 3.20 – A: PPy TGA curve; B: Derivative of the PPy TGA curve.

Regarding PPy thermal decomposition pattern (**Figure 3.20**), dehydration is visible at 100 ºC being this event followed by a slight weight loss due to the removal of small PPy oligomers. Finally, it is visible that the PPy suffers a long single-step decomposition which occurs between 250-650 ºC which correspond to the breakage of the polymer chains and subsequent vaporisation of smaller fragments such as Py dimers and such.

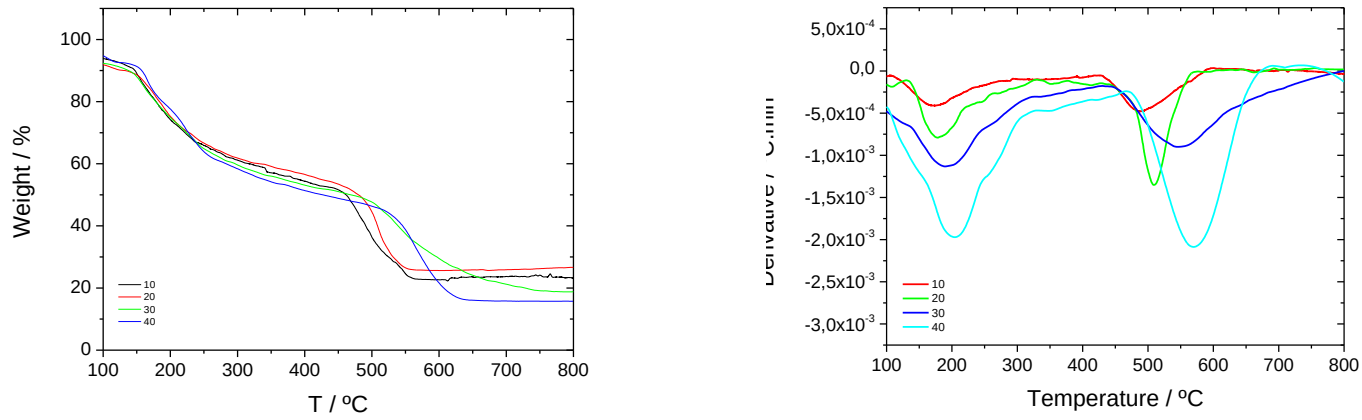

Figure 3.21 – A: BC-PPy TGA curve; B: Derivative of the BC-PPy TGA curve.

The thermogram of the BC-PPy composites (**Figure 3.21**) is a combination of the patterns of both BC and PPy as it can better observed on **Figure 3.22** which summarizes the three profiles, BC, PPy and BC-PPy.

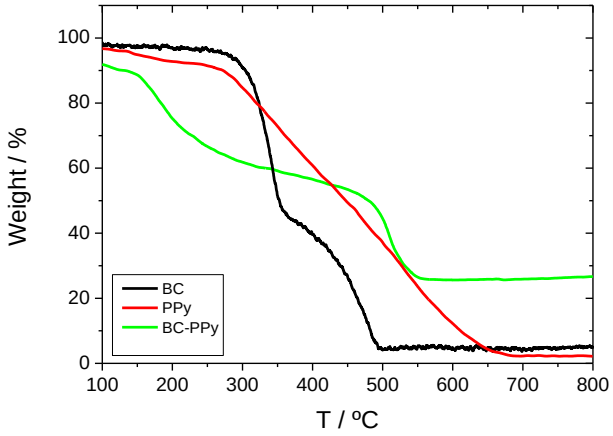

Figure 3.22 –TG curves for all the analysed materials.

These composites, similary to the BC, display a multi-step thermal decomposition with two steps at 150-350 ºC and 430-650 ºC. The first step corresponds to the degradation of small PPy and BC oligomers, however, it is noteworthy that this step is quite less steep than the one on the BC thermogram, despite beginning at a lower temperature. This is due to the presence of the PPy that coats the fibres, which apparently improve the material's thermal stability thus broadening the decomposition step on the graph hence looking more alike to the PPy thermogram.

Finally, the second step represents the rupture of the BC polymeric chains and of PPy residues. This step is very similar to the one on the BC thermogram despite occurring at a slightly higher temperature range which can be related to the stabilization of the material's thermal stability by the presence of PPy.

Along with the previous observations, on the BC-PPy composites thermogram a relatively high % of residual mass exists, accounting for approximately 25% of the total mass of the samples. This residue is solely composed of iron particles that are not vaporised (as iron is only vaporised past 2862 ºC), which originate from the $FeCl_3$ used during the oxidation step. Since relatively high quantities of $FeCl_3$ were used in these

experiments, it is natural that an appreciable amount of oxidized iron particles powder is found on the crucible (**Figure 3.23**), following the TGA assays**.**

Figure 3.23 – Top view photograph of the crucible with the iron residue left after the analysis of the BC-PPy composites.

Thermal degradation kinetics

Regarding the thermal degradation kinetics, the energy of activation (E_{act}) was calculated for the samples using the Kissinger's Method. A Kissinger's plot was elaborated by plotting the logarithm of the heat rate dividing by the squared T_{max}, obtained through the derivatives (**Figures 3.19B, 3.20B** and **3.21B**), *vs* the inverse temperature, in Kelvin. A linear regression is then applied to the graph and the slope of the linear regression line corresponds to the E_{act} of the compound. **Figures 3.25** represents the Kissinger's plots and respective linear regressions for the BC's first and second steps respectively.

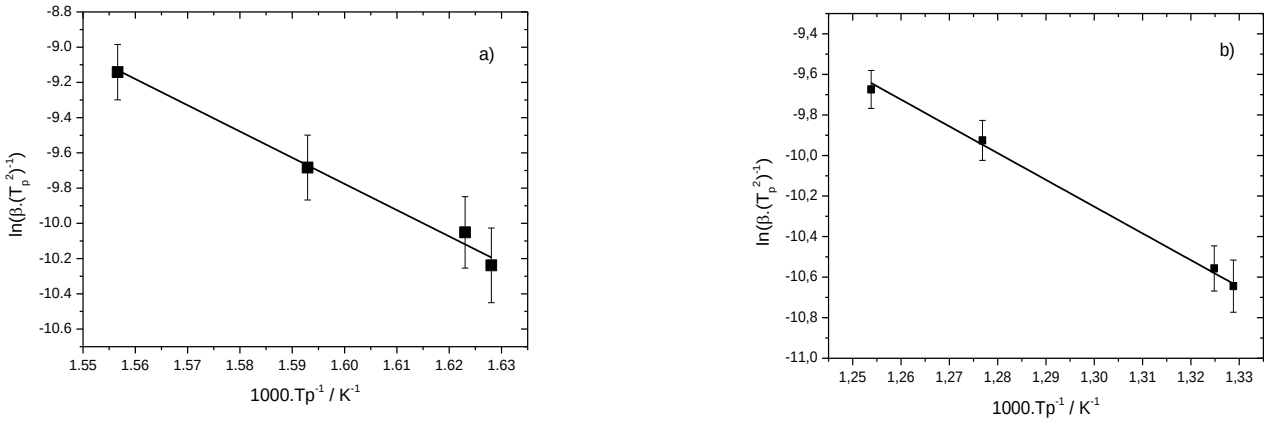

Figure 3.24 – Kissinger plot for the BC thermal degradation and respective linear regression for E_{act} calculus for both first (a) and second (b) thermal decomposition steps.

The calculated E_{act} values, as well as the medium residue found on the end of the TGA runs are displayed in **Table 3.3:**

Table 3.3 – TGA parameters and thermal decomposition kinetics of BC, PPy and BC-PPy composites.

Samples		1	2
	Residue / %	E_{act} / kJ.mol-1	
BC	4.128 ± 1,76	123.7 ± 6.4	109.1 ± 5.4
PPy	3.625 ± 1.81	113.5 ± 7.1	-
BC-PPy	21.14 ± 4.81	190.8 ± 10.4	68.6 ± 3.2

Regarding the activation energies, values from **Table 3.3** reinforce the impact that the incorporation of PPy onto the BC matrix had towards the thermal stability of the composite as in the first step, a higher amount of energy is required for the material's degradation to occur. Additionally, the TG curve (**Figure 3.22**) shows that the first step is less steep comparatively to the original materials which indicates that more time at higher temperatures is required to degrade the sample hence the higher E_{act} values.

The second step, by its turn, displays a fairly lower energy of activation comparatively to BC. Once again the observation of the TG curve (**Figure 3.22**) corroborates with these results as the second degradation step for the BC-PPy composites is slightly steeper than the one for the BC which indicates that the material is vaporised faster possibly due to decreased thermal stability of the fibres caused by the modification made by the PPy deposition.

Chapter 4. Conclusions and future work

Throughout the course of this research, electrically conductive composites were successfully obtained by using the chemical vapour deposition of PPy onto the BC fibre matrix. This was achieved by using the wet chemical polymerization and chemical vapour methods. The effect of the usage of never-dried BC *vs* freeze-dried BC towards the conductivity of the composites was also assessed.

The electrical conductivities range between $3x10^{-5}$ to $5x10^{-5}$ $S.m^{-1}$, for the CVD, and 3-140 $S.m^{-1}$, for the WCP, being the highest values obtained after the longest reaction time.

The obtained composites were submitted to a detailed physicochemical characterization using analytical techniques such as FTIR-ATR, TGA, SEM, tensile testing, XRD and electrical conductivity measures. All the performed analysis revealed, concordantly, that the BC fibres were successfully coated with a PPy layer being this layer visible on the SEM micrographs and confirmed by both FTIR-ATR and XRD. Regarding the FTIR-ATR, the BC-PPy composites IR spectrum shares peaks between the BC and the PPy, and XRD reveals that BC crystallinity decreases with the PPy *in situ* polymerization.

Finally, both thermal and mechanical properties of the composites are slightly different from the pristine materials being an increment in thermal stability verified when compared to both BC and PPy and an abrupt decay on the mechanical properties comparatively to the BC. It is highly likely that these differences are related to the deterioration of the fibres due to both the oxidative treatment and the deposition of PPy and its consequent chemical interactions with the BC fibres.

There is, however, plenty of future work ahead of this research which, by its turn, consists of further optimisation of the synthesis methods, namely on the CVD method, where the PPy excessive accumulation on the BC membrane's surface must be avoided in order to attain higher conductivities. The interaction between the fibres and the PPy can also be studied more thoroughly in order to explain the remarkable changes on both thermal and mechanical properties.

Relatively to the application potential of these composites, a variable set of applications can already undergo an initial development stage. The tailor-made conductivity exhibited by these composites broadens the areas where these composites can be introduced. For example, the cBC-PPy composites can be used on the development of sensors and on nervous cell growth with electrical stimuli as they have fairly low conductivity which is enough to conduct well the electric current but not high enough to kill the cells by excessive heat dissipation. However, it is crucial to use a different oxidizing agent for the polymerisation as $FeCl_3$ is cytotoxic. A good starting-point would be the use of Ammonium Persulfate (APS) which is a cytocompatible oxidizing agent (Muller *et al.* 2013). The wBC-PPy composites, by their turn, can be employed on the development of applications such as super-capacitors (Wang *et al.*, 2013) and flexible electronics due to germanium and silicon-levels of conductivity, being these elements commonly used on the development of electronic devices and e-paper applications, being this the main focus in the future.

The major drawback of the usage of these composites towards the development of this type of applications is, currently, their mechanical properties which lead to poor processability. However, this issue can be obviated by using an alternate solvent as when water is used, despite yielding composites with very high conductivities, the mechanical properties of the material are remarkably worse. Some good examples of solvents that can be tested are acetonitrile and ethylene glycol which may not hinder the mechanical properties as much. Ultimately, this problem can be overcome by reinforcing the mechanical resilience of the material by coating it with silicone rubber, among other elastic polymers, which will possibly result in its increased mechanical endurance while keeping its main intrinsic property – its electrical conductivity.

In conclusion, the main objective of this work was the synthesis of electrically composites through *in situ* polymerisation of PPy on the BC was achieved. The effect of using freeze-dried BC was also assessed and verified to be impactful as a high increase in the composite's electrical conductivity. As regards to the implementation of the CVD, it is possible to conclude that while this technique is successful towards the BC-PPy composite synthesis it still lacks optimisation. It is also noteworthy that, despite the obtained composites properties not being completely comparable with the prime

materials, *i.e.* conductivities as high as pure PPy (500 $S.m^{-1}$) and the tensile strength and Young's modulus of the BC, these composites have intermediate characteristics between their prime materials.

Bibliography

Aldissi, M. (1984). Review Of The Synthesis Of Polyacetylene And Its Stabilization To Ambient Atmosphere. *Synthetic Metals*, 9(2), 131-141.

Al-Mashat, L., Tran, H. D., Wlodarski, W., Kaner, R. B., & Kalantar-zadeh, K. (2008). Polypyrrole Nanofiber Surface Acoustic Wave Gas Sensors. *Sensors and Actuators B: Chemical*, 134(2), 826-831.

Andrade, F. K., Pertile, R. A., Dourado, F., & Gama, F. M. (2010). Bacterial cellulose: Properties, Production and Applications.. *Cellulose: structure and properties, derivatives and industrial uses*(pp. 427-458). NY: Lejeune, A..

Anjos, B., Novaes, A. B., Meffert, R., & Barboza, E. P. (1998). Clinical comparison of cellulose and expanded polytetrafluoroethylene membranes in the treatment of class II furcations in mandibular molars with 6-month re-entry.. Journal of Periodontology, 69 (4), 454-459.

Ansari, R. (2006). Polypyrrole Conducting Electroactive Polymers: Synthesis and Stability Studies. E-Journal of Chemistry, 3(4), 186–201.

Arbia, W., Arbia, L., Adour, L., & Amrane, A. (2012). Chitin Extraction from Crustacean Shells by Biological Methods – A review. (n.a.), (n.a.), (n.a.).

Babu, K. F., Dhandapani, P., Maruthamuthu, S., & Kulandainathan, M. A. (2012). One pot synthesis of polypyrrole silver nanocomposite on cotton fabrics for multifunctional property. Carbohydrate Polymers, 90, 1557–1563.

Bäckdahl, H., Esguerra, M., Delbro, D., Risberg, B., & Gatenholm, P. (2008). Engineering Microporosity In Bacterial Cellulose Scaffolds. Journal of tissue engineering and regenerative medicine,2(6), 320-330.

Bagavathiappan, S., Saravanan, T., Philip, J., Jayakumar, T., Raj, B., Karunanithi, R., et al. (2008). Investigation Of Peripheral Vascular Disorders Using Thermal Imaging. The British Journal of Diabetes & Vascular Disease, 8(2), 102-104.

Bakhshi, A.; Bhalla, G. (2004). Electrically conducting polymers: Materials of the twenty-first century. Journal of Scientific & Industrial Research. 63, p715-728.

Barrios, V. A., Méndez, J. R., Aguilar, N. V., Espinosa, G. A. and Rodríguez J. L. (2012). FTIR - An Essential Characterization Technique for Polymeric Materials, Infrared Spectroscopy - Materials Science, Engineering and Technology, Prof. Theophanides Theophile (Ed.), ISBN: 978-953-51-0537-4, InTech

Beneventi, D.; Alila, S.; Boufi, S.; Chaussy, D.. (2006). Polymerization of pyrrole on cellulose fibres using a FeCl 3 impregnation-pyrrole polymerization sequence. Cellulose. 13, p725-734.

Bidez, P. R., Li, S., MacDiarmid, A. G., Venancio, E. C., Wei, Y., & Lelkes, P. I. (2006). Polyaniline, An Electroactive Polymer, Supports Adhesion And Proliferation Of Cardiac Myoblasts.Journal of Biomaterials Science, Polymer Edition, 17(1), 199-212.

Borthakur, L. J., Konwer, S., Das, R., & Dolui, S. K. (2011). Preparation of conducting composite particles of styrene–methyl acrylate copolymer as the core and graphite-incorporated polypyrrole as the shell by surfactant-free mini emulsion polymerization.Journal of Polymer Research, 18, 1207-1215.

Brown, A. J. (1886). The Chemical Action Of Pure Cultivations Of Bacterium Aceti. Journal of the Chemical Society, Transactions, 49, 172.

Cellulose (plant cell structure) -- Encyclopedia Britannica. (n.d.).Encyclopedia Britannica. Retrieved October 7, 2013, from http://www.britannica.com/EBchecked/topic

Cheng, H.; Wang P.; Chen J.; Wu W.. (2002). Cultivation of Gluconacetobacter xylinus for bacterial cellulose production in a modified airlift reactor. Biotechnol. Appl. Biochem.. 35, p125-132.

Cheng, K., Catchmark, J. M., & Demirci, A. (2009). Enhanced Production Of Bacterial Cellulose By Using A Biofilm Reactor And Its Material Property Analysis. Journal of biological engineering, 3(1), 12.

Chiang, C. K., Druy, M. A., Gau, S. C., Heeger, A. J., Louis, E. J., MacDiarmid, A. G., et al. (1978). Synthesis Of Highly Conducting Films Of Derivatives Of Polyacetylene, (CH)x. Journal of the American Chemical Society, 100(3), 1013-1015.

Chiang, C. K., Fincher, C. R., Park, Y. W., & Heeger, A. J. (1977). Electrical Conductivity In Doped Polyacetylene.Physical Review Letters, 39(17), 1098-1101.

Coats, A. W., & Redfern, J. P. (1963). Thermogravimetric Analysis. A Review.The Analyst, 88(1053), 906.

Dall'acqua, L., Tonin, C., Varesano, A., Canetti, M., Porzio, W., & Catellani, M. (2006). Vapour Phase Polymerisation Of Pyrrole On Cellulose-based Textile Substrates. Synthetic Metals, 156(5-6), 379-386.

electrical conductivity: range of conductivity -- Encyclopedia Britannica. (n.d.). Encyclopedia Britannica. Retrieved October 9, 2013, from http://www.britannica.com/EBchecked/media/139/Typical-range-of-conductivities-for-insulators-semiconductors-and-conductors

Fontana, J. D., Bichara, J. A., Narcisco, G. P., Souza, S. J., Gallotti, B. J., Moreschi, J. C., et al. (1990). Acetobacter Cellulose Pellicle As A Temporary Skin Substitute.Applied Biochemistry and Biotechnology,24-25(1), 253-264.

Gostomski, P; Bungay, H; Mormino, R. (2002). Plate and disk bioreactors for making bacterialcellulose. Biological Systems Engineering, 830, 69-78.

Helenius, G., Bäckdahl, H., Bodin, A., Nannmark, U., Gatenholm, P., & Risberg, B. (2006). In Vivo Biocompatibility Of Bacterial Cellulose. Journal of Biomedical Materials Research Part A, 76A(2), 431-438.

Hornung, M., Ludwig, M., & Schmauder, H. (2007). Optimizing The Production Of Bacterial Cellulose In Surface Culture: A Novel Aerosol Bioreactor Working On A Fed Batch Principle (Part 3). Engineering in Life Sciences, 7(1), 35-41.

Iguchi, M; Mitsuhashi, S; Ichimura, K; Nishi, Y; Uryu, M; Yamanaka, S; Watanabe, K.. Bacterial cellulose-containing molding material having high dynamic strength. US 4742164 A, 1998.

Iguchi, M; Yamanaka, S; Budhiono, A. (2000). Bacterial cellulose - a masterpiece of nature's arts. Journal of Materials Science, 35, (2), 261-270.

Indrartil, L., Yudiantil, R., Amurwabumil, K., Jurnal, N. Y. (1998). Application of biocellulose as an acoustic membrane, Indonesian Journal of Biotechnology, 6: 180-184.

Infrared Spectroscopy - Materials Science, Engineering and Technology, Prof. Theophanides Theophile (Ed.), ISBN: 978-953-51-0537-4, InTech

Jin, Z.; Su, Y.; Duan, Y. (2000). An improved optical pH sensor based on polyaniline. Sensors and Actuators B: Chemical. 71 (1), P118-122.

Jonas, R.; Farah, L. F. (1998). Production and application of microbial cellulose. Polymer Degradation and Stability. 59, p101-106.

Kissinger, H. E.Reaction (1957). Reaction Kinetics in Differential Thermal Analysis. A*nal. Chem.*, *29* (11), pp 1702–1706

Klemm, D; Schumann, D; Udhardt, U; Marsch, S. (2001). Bacterial synthesized cellulose -artificial blood vessels for microsurgery. Progress in Polymer Science, 26, (9), 1561-1603.

Lapuz, M. M.; Gallardo, EG; Palo, M. A. (1967). The nata organism - cultural requirements, characteristics and identity. The Phillippine Journal of Science, 96, (2), 91-109.

Legnani, C., Vilani, C., Calil, V., Barud, H., Quirino, W., Achete, C., et al. (2008). Bacterial Cellulose Membrane As Flexible Substrate For Organic Light Emitting Devices. Thin Solid Films, 517(3), 1016-1020.

Linford, R. G. (1990). Electrochemical science and technology of polymers-2. (n.d.): Springer.

Macasaquit, A., & Binag, C. (2010). Preparation of Conducting Polyester Textile by in situ Polymerization of Pyrrole. Philippine Journal of Science ,139(2), 189-196.

MacDiarmid, A. G. (2001). “Synthetic Metals”: A Novel Role For Organic Polymers (Nobel Lecture). Angewandte Chemie International Edition, 40(14), 2581-2590.

MacDiarmid, A. G., Mammone, R. J., Kaner, R. B., Porter, S. J., Pethig, R., Heeger, A. J., et al. (1985). The Concept Of `Doping' Of Conducting Polymers: The Role Of Reduction Potentials [and Discussion]. Philosophical Transactions of the Royal Society A: Mathematical, Physical and Engineering Sciences,314(1528), 3-15. MacDiarmid, A. G., Mammone, R. J., Kaner, R. B., Porter, S. J., Pethig, R., Heeger, A. J., et al. (1985). The Concept Of `Doping' Of Conducting Polymers: The Role Of Reduction Potentials [and Discussion]. Philosophical Transactions of the Royal Society A: Mathematical, Physical and Engineering Sciences,314(1528), 3-15.

Machida, S. (1989). Chemical Synthesis Of Highly Electrically Conductive Polypyrrole. Synthetic Metals, 31(3), 311-318.

Markiewics, E.; Hilczer, B.; Pawlaczyk, C.. (2004). Dielectric and Acoustic Response of Biocellulose. Ferroelectrics. 304, p39-42

Masaoka, S., Ohe, T., & Sakota, N. (1993). Production Of Cellulose From Glucose By Acetobacter Xylinum. Journal of Fermentation and Bioengineering,75(1), 18-22.

Mayer, R.; Ross, P; Weinhouse, H.; Amikam, D.; Volman, G.; Ohana, P.; Calhoon, R. D.; Wong, H. C.; Emerick, A. W.; Benziman, M.. (1991). Polypeptide composition of bacterial cyclic diguanylic acid-dependent cellulose synthase and the occurrence of immunologically crossreacting proteins in higher plants. Proc. Nati. Acad. Sci.. 88, p5472-5476.

McChesney J.D., Venkataraman S.K., Henri J.T. (2007). Plant natural products: Back to the future or into extinction? Phytochemistry, 68: 2015-2022.

McMullan, D. (1989). SEM - past, present and future. Journal of Microscopy, 155(3), 373-392.

Membranes, Journal of Macromolecular Science, Part B, 51:3, 411-424

Miyamoto T, Takahashi S, Ito H, Inagaki H, Noishiki Y. (1989). Tissue biocompatibility of cellulose and its derivatives. J Biomed Mater Res, 23, 125–133.

Moosavi-Nasab, M., and A. R. Yousefi. "Investigation of Physicochemical Properties of the Bacterial Cellulose Produced by Gluconacetobacter xylinus from Date Syrup." World Academy of Science, Engineering and Technology 44 (2010): 1258-1263. Print.

Mormino, R; Bungay, H. (2003) Composites of bacterial cellulose and paper made with arotating disk bioreactor. Applied Microbiology and Biotechnology, 62, (5-6), 503-506.

Muller, D., Rambo, C. R., Porto, L. M., Schreiner, W. H., & Barra, G. M. (2013). Structure and properties of polypyrrole/bacterial cellulose nanocomposites. Carbohydrate Polymers,94, 655-662.

Nambiar, S.; Yeow, J. T. W.;. (2011). Conductive polymer-based sensors for biomedical applications. Biosensors and Bioelectronics . 26 (1), p1825-1832.

Nguyen, V., Gidley, M., & Dykes, G. (2008). Potential Of A Nisin-containing Bacterial Cellulose Film to Inhibit Listeria Monocytogenes On Processed Meats.Food Microbiology, 25(3), 471-478.

Nogi, M., Abe, K., Handa, K., Nakatsubo, F., Ifuku, S., & Yano, H. (2006). Property Enhancement Of Optically Transparent Bionanofiber Composites By Acetylation.Applied Physics Letters, 89(23), 233123.

Okiyama, A., Motoki, M., & Yamanaka, S. (1992). Bacterial Cellulose II. Processing Of The Gelatinous Cellulose For Food Materials. Food Hydrocolloids, 6(5), 479-487.

Okiyama, A., Motoki, M., & Yamanaka, S. (1993). Bacterial Cellulose IV. Application To Processed Foods. Food Hydrocolloids,6(6), 503-511.

Pértile, R. A. N.; Siqueira, J. M.; Rambo, C. R.; Berti, F. V.; do Valle, R. M. R.; Porto, L. M. (2007). Interação de cultura celulares com suportes biopoliméricos para aplicações biomédicas. Exacta, 5, (2), 343-352.

Ribelles & S. Lanceros-Mendez (2012): Thermal Properties of Electrospun Poly(Lactic Acid)

Sanchavanakit, N., Sangrungraungroj, W., Kaomongkolgit, R., Banaprasert, T., Pavasant, P., & Phisalaphong, M. (2006). Growth Of Human Keratinocytes And Fibroblasts On Bacterial Cellulose Film.Biotechnology progress, 22(4), 1194-1199.

Saville, P.. (2005). Polypyrrole Formation and Use. Defence R&D Canadax-Atlantic. , p1-5.

Schostek, S.; Schurr, M. O.; Buess, G. F. (2009). Review on aspects of artificial tactile feedback in laparoscopic surgery. Medical Engineering & Physics. 31 (8), p887-898.

Schramm, M.; Hestrin, S.. (1954). Factors affecting Production of Cellulose at the Air/Liquid Interface of a Culture of Gluconacetobacter xylinus. J. gen. Microbiol. 11, p123-129.

Shah, J; Brown, R.M. (2005). Towards electronic paper displays made from microbial cellulose. Applied Microbiology and Biotechnology, 66, (4), 352-355.

Surma-Slusarska, B; Presler, S; Danielewicz, D. (2008). Characteristics of bacterial cellulose obtained from Gluconacetobacter xylinus culture for application in papermaking. Fibres & Textiles in Eastern Europe, 16, (4), 108-111.

US Congress, Office of Technology Assesment (1993). Biopolymers: making materials nature´s way-background paper, OTA-BP-E-02. In US Government Printing Office: Washington, DC, 59-60.

V. Sencadas, C. M. Costa, G. Botelho, C. Caparrós, C. Ribeiro, J. L. Gómez-

Vaitkuviene, A., Kaseta, V., Voronovic, J., Ramanauskaite, G., Biziuleviciene, G., Ramanaviciene, A., & Ramanavicius, A. (2013). Evaluation of cytotoxicity of polypyrrole nanoparticles synthesized by oxidative polymerization. Journal of hazardous materials, 250-251, 167–74.

Valla, S., & Kjosbakken, J. (1982). Cellulose-negative Mutants of Acetobacter xylinum. Microbiology, 128(7), 1401–1408.

Vernitskaya, T. V., & Efimov, O. N. (1997). Polypyrrole: A Conducting Polymer; Its Synthesis, Properties And Applications. Russian Chemical Reviews,66(5), 443-457.

Wang, H., Bian, L., Zhou, P., Tang, J., & Tang, W. (2013). Journal of Materials Chemistry. Core–sheath structured bacterial cellulose/polypyrrole nanocomposites with excellent conductivity as supercapacitors†, 1, 578-584.

Warren, B. E. (1969). X-ray diffraction. Reading, Mass.: Addison-Wesley Pub. Co..

Watanabe, K; Eto, Y; Takano, S; Nakamori, S; Shibai, H; Yamanaka, S. (1993). A New Bacterial Cellulose Substrate for Mammalian-Cell Culture - a New Bacterial Cellulose Substrate. Cytotechnology, 13, (2), 107-114.

Xue, X., Deng, P., Yuan, S., Nie, Y., He, B., Xing, L., et al. (2013). CuO/PVDF nanocomposite anode for a piezo-driven self-charging lithium battery. Energy & Environmental Science, 6, 2615-2620.

Yano, H; Sugiyama, J; Nakagaito, AN; Nogi, M; Matsuura, T; Hikita, M; Handa, K. (2005). Optically transparent composites reinforced with networks of bacterial nanofibers. Advanced Materials 2005, 17, (2), 153-+.

Zuo, K.; Cheng, H.; Wu, S.; Wu, W.. (2006). A hybrid model combining hydrodynamic and biological effects for production of bacterial cellulose with a pilot scale airlift reactor. Biochemical Engineering Journal. 29, p81-90.